A COMPREHENSIVE FRAMEWORK FOR IMAGE GUIDED BREAST SURGERY

By

Rebekah H. Conley

Thesis

Submitted to the Faculty of the

Graduate School of Vanderbilt University

in partial fulfillment of the requirements

for the degree of

MASTERS OF SCIENCE

in

BIOMEDICAL ENGINEERING

May, 2015

Nashville, Tennessee

Approved:

Professor Michael I. Miga, Ph.D.

Professor Robert L. Galloway, Ph.D.

ACKNOWLEDGMENTS

I will start out by thanking the current and former members of the Biomedical Modeling Laboratory at Vanderbilt, especially Dr. Tom Pheiffer for his guidance and help with the ultrasound data, Jarrod Collins for help with data acquisition, Dr. Jared Weis for help with understanding and implementing the biomechanical model, and Yifei Wu for helpful discussions and assistance with data acquisition.

I would like to acknowledge the Vanderbilt Initiative in Surgery and Engineering Pilot Award Program for support of this work. This work was supported in part by a National Science Foundation Graduate Research Fellowship. This work was also partially funded by CTSA award No. UL1TR000445 from the National Center for Advancing Translational Sciences.

Next, I would thank Dr. Lori Arlinghaus-Davis for her crucial help in producing quality supine MR images. I would also like to acknowledge Dr. Ingrid Meszoely for her encouragement and overall enthusiasm to work with me to obtain real breast cancer patient data. I want to thank Dr. Thomas Yankeelov for his guidance and support while keeping meetings fun and entertaining. I would like to extend my gratitude to my adviser, Dr. Miga, for working with me to initialize this project and for providing guidance for without this project would not have succeeded.

Finally, I would like to thank my family and friends for their continued support and encouragement throughout this process, especially my parents and my fiancé, Andy.

TABLE OF CONTENTS

LIST OF FIGURES

LIST OF ABBREVIATIONS

BCT Breast Conserving Therapy

MR Magnetic Resonance

MRI Magnetic Resonance Image

OR Operating Room

ROLL Radioguided Occult Lesion Localization

RSL Radio-guided Seed Localization

preOp Preoperative

intraOp Intraoperative

US Ultrasound

iUS intraoperative Ultrasound

FEM Finite Element Method

ICP Iterative Closest Point

FRE Fiducial Registration Error

PCA Principal Component Analysis

MIE Modality Independent Elastography

CHAPTER I

Introduction

I.0.1 Motivation

Breast cancer is the most frequently diagnosed cancer and the leading cause of cancer related deaths among females worldwide (Torre et al., 2015). In the United States, breast cancer is the second most commonly diagnosed cancer among women and a leading cause of cancer related deaths, second only to lung cancer (DeSantis et al., 2014). A woman living in the United States has a 1-in-8 lifetime risk of being diagnosed with breast cancer. Approximately 232,340 new cases of invasive breast cancer were diagnosed in the U.S. in year 2013. In addition, approximately 64,640 new diagnosed cases of in situ breast cancers occurred in 2013 (DeSantis et al., 2014). Breast cancer is a complex and heterogeneous disease with multimodal approaches for treatment. Initial treatment of primary breast tumors is usually surgical. Surgical options include mastectomy (total removal of the breast) and breast conservation therapy (BCT). BCT consists of removal of the tumor with 0.5-1 cm margin of normal tissue combined with radiation therapy. Mastectomy was the most common procedure choice for newly diagnosed breast cancer patients until the 1980s when studies revealed that lumpectomy, the far less disfiguring option, was shown to have the same 10 year survival rate as mastectomy (Fisher et al., 1985). Recently, an increasing trend towards the use of mastectomy has been recorded in the United States (Lucas et al., 2015) despite BCT being the preferred method of therapy with recent studies showing higher breast-cancer specific survival rates when compared to mastectomy (Agarwal et al., 2014). The reasons for increased mastectomy rates are complex and not fully understood but may include improvements in mastectomy techniques, access to reconstruction, increasing use of genetic testing, preoperative MRI findings, and other patient-related fears and anxieties about recurrence or repeat surgeries (Sledge et al., 2014).

A substantial concern for a BCT eligible patient is whether or not negative margins will be achieved during the initial surgery. Negative margins are achieved when no cancer cells are within a 0.5-1 cm margin of the excised tissue. Unfortunately, the reoperation rates due to lumpectomy margin status averages 20-40% (Landercasper et al., 2014). The European Union of Breast Cancer Specialists (EUSOMA) endorse a minimum standard of 80% and a target of 90% success rate of first time surgeries as a quality of care metric (Del Turco et al., 2010). Second and third operations reported in breast surgery are disproportionately high compared with other general surgery practices (Eck et al., 2012). Reoperations cause a host of problems including emotional and financial stress on the patient as well as an increase in the public healthcare burden.

Other consequences of failing to achieve negative margins during the initial surgery include delay of post-operative radiation treatment and chemotherapy, increase risk for local recurrence, and compromises in the cosmetic outcome. Thus, reducing the rate of secondary operations for margin re-excision or full mastectomy has benefits that are patient-centered and cost-effective.

Avoiding reoperations due to positive margins can be difficult. A significant amount of BCT surgical cases involve non-palpable tumors (Eck et al., 2012). This requires the surgeon to rely on radiographic information and techniques to guide lesion excision. The challenge in determining surgical margins intraoperatively is that geometric and spatial cues are quickly lost in the surgical presentation. Equally confounding is that valuable diagnostic images are acquired in significantly different breast presentations than the typical surgical setup. Diagnostic and biopsy information are driven by mammography and preoperative MR images in which the patient is standing or lying prone with pendulous breasts, while surgical presentation is in the supine position. This presents a limitation in the use of preoperative MR images to guide surgical excision.

The motivation of this work lies in the need to improve lumpectomy procedures to decrease reoperation rates. Superior ability to localize tumors and delineate borders intraoperatively has the potential to decrease the incidence of positive margins. Currently, the under-utilization of MR data in the operating room (OR) could be remedied by acquiring supine MR images that more closely represent surgical orientation and registering them to patient space. Therefore, the development of an image guidance system using supine MRI to guide lumpectomy procedures could address the need of superior localization strategies.

I.0.2 Previous Work in Intraoperative Tumor Localization

I.0.2.1 Current Methods

Historically, wire guided localization has been the standard technique for localizing non-palpable or clinically occult breast lesions intraoperatively. Wire guide localization consists of introducing a wire into the tumor under the guidance of mammography, ultrasound, or MRI. The wire consists of an anchor located at the distal end to avoid dislodging the wire during the time between wire placement and surgery. This wire then protrudes out from the breast surface until the patient is taken into the operating room. Once there, the surgeon identifies the wire trajectory using the preoperative mammogram or intraoperative ultrasound. A plan is then made to resect tissue along the trajectory of the wire stopping 1-2 cm before the distal end. Once here, the surgeon will change direction to dissect around the wire tip while taking care to avoid penetrating into the cancerous lesion. Once excised, the specimen is inked using various colors or sutured to designate the anatomical orientation of the specimen and analyzed for positive margin status. This specimen should contain the wire tip, biopsy clip, calcifications, and tumor with a surrounding margin of healthy tissue.

This technique has been criticized in the last several years due to the inexact nature of the procedure and

high rates of positive margins (38-43%) (Allweis et al., 2008; Tafra et al., 2006). An obstacle surrounding the use of wire guide localization is that the guide wire does not provide a 3D perspective of the tumor and therefore cannot delineate tumor borders. In some cases, the trajectory of the wire is dictated by mammographic guidance and can represent inefficient surgical routes to the target which would direct the surgeon to navigate through excessive amounts of tissue or require the surgeon to make a visual estimation of a better route, both potentially leading to poor outcomes in regards to cosmesis and a clean excision. Other problems that occur with wire guide localization include off target placement of the wire and dislodgement/movement of the wire prior to or during the surgical procedure due to specimen manipulation.

Intraoperative ultrasound is commonly used and has shown to improve BCT (Davis et al., 2011). However, the use of intraoperative ultrasound is limited by the fact that only 50% of non-palpable tumors are visible by ultrasound in the breast (Klimberg, 2003). More recently, radioguided occult lesion localization (ROLL) and radio-guided seed localization (RSL) have shown promise to improve localization of clinically occult lesions. Specifically, ROLL has shown to reduce the incidence of positive margins when compared to wire-guide localizations (van Esser et al., 2008). The ROLL technique injects a radioisotope into the tumor under stereotactic or ultrasound guidance. The location of the tumor can then be found using a hand-held gamma probe. The gamma probe can also be used to locate areas of higher radioactivity following excision of the tumor to identify potential remnant tumor cells. The shortcomings of radio-guided occult lesion localization is that the radioisotope must be accurately placed into the tumor and diffusion of the radiotracer into surrounding tissue decreases accuracy of the tumor location (van Esser et al., 2008). RSL is similar to ROLL except for a radioactive seed is introduced into the tumor prior to surgery. RSL cannot provide a 3D delineation of tumor borders. Both ROLL and RSL rely upon accurate injection/placement of the radioisotope under image guidance. While used in many breast cancer centers, RSL and ROLL techniques have yet to be widely adopted.

I.0.2.2 Surgical navigation with preoperative MRI

The use of preoperative MR images for surgical planning has historically been controversial. Previous studies report that retrospective data and randomized trials have not shown preoperative MRI to reduce re-excisions, lower recurrence rates, or improve survival benefits (Peters et al., 2011; Hwang et al., 2009; Turnbull et al., 2010; Chandwani et al., 2014; McGhan et al., 2010; Bleicher et al., 2009). Many argue that preoperative MRI is associated with an increase in the use of mastectomy, delay in treatment, and an increase in the number of additional biopsies (Kuhl et al., 2007; Houssami et al., 2008; Turnbull et al., 2010) and therefore should not be routinely used for preoperative planning purposes. Alternatively, several studies have disputed these claims arguing that MRI provides invaluable information regarding the extent of disease. A recent

prospective, randomized, multicenter study reports a significant decrease in reoperation rates between women who received a preoperative staging MRI vs. women who did not receive an MRI prior to lumpectomy (Gonzalez et al., 2014). Sung et al. (2014) published a retrospective analysis that concluded that reoperation rates among BCT patients were lower for women who received a preoperative MRI. Several other studies report positive findings for improved preoperative staging using MRI (Esserman et al., 1999; Fischer et al., 2004; Braun et al., 2008; Sung et al., 2014; Gonzalez et al., 2014)

Overall, the argument surrounding the value of preoperative MRI remains inconclusive. However, it is generally agreed upon that MRI provides the most accurate delineation of the size and extent of cancer and offers the highest sensitivity for intraductal extensions involved in invasive cancers. A common criticism of arguments against the use of preoperative MRI is how the images are presented to the surgeon for guidance. As previously discussed, preoperative MR images are acquired in the prone position with pendulous breasts while surgery is performed with the patient lying supine. Several studies have reported significant displacements in breast tumors between the prone and supine positions on the order of 18-60 mm (Pallone et al., 2014; Satake et al., 2014; Carbonaro et al., 2012). These relatively large displacements render prone MR images sub-optimal for use in surgical planning and navigation, which may contribute to studies finding little to no benefit of preoperative MRI.

Due to these realizations, several groups have investigated the use of preoperative MR images rendered in positions that more closely represent the surgical orientation. Prone-to-supine registration methods of MR images for use in image guided breast surgery have been developed (Han et al., 2014b, 2011; Eiben et al., 2013; Carter et al., 2006b, 2008; Rajagopal et al., 2008; Carter et al., 2006a) . A more direct approach is to use supine MR images to direct surgery, which has been explored by several groups. Tozaki and Fukuda (2006) reported that acquiring preoperative supine MR images may be useful for the planning of breast conservation therapy. A new approach to breast conserving surgery that uses a projection technique to reproduce an outline of the lesion on the breast surface using the location of the tumor based on the preoperative supine MRI was described in Sakakibara et al. (2008). Yamashiro et al. (2009) presented a technique that uses supine MRI to modify resection lines for tumors with unclear margins by ultrasound. Abe et al. (2011) made use of a thermoplastic shell to reproduce the preoperative breast shape in the OR to mark the location of the tumor based on the preoperative supine MRI. Intraoperative MRI for breast cancer surgery was evaluated by Golshan et al. (2014). However, intraoperative MRI surgical suites are not present in most hospitals across the U.S.

Registration of preoperative supine MR images to physical space in the operating room for MRI navigated breast surgery has been another avenue of development. Frameworks using prone-to-supine registration followed by supine image to physical space registration have been described (Carter et al., 2006b, 2008). Alderliesten et al. (2010) used preoperative supine MR images and optical tracking technology to quantify

needle tip position uncertainty for radioactive seed localization procedures and demonstrated that using pre-operative supine MR to demarcate breast cancer in the operating room is feasible. Alignment of pre-surgical supine MR images to surgically oriented MR images using surface markers has been shown to be feasible (Ebrahimi et al., 2014). Preoperative supine MR images registered using surface markers coupled with an intraoperative optical scan of the breast has also demonstrated qualitative alignment value (Pallone et al., 2014). While developments in image guided surgical systems for breast cancer surgeries have been encouraging, the integration of supine MR images, optical tracking and digitization technology, patient specific biomechanical models for nonrigid registration, and tracked ultrasound for subsurface feature localization have yet to be realized as a surgical guidance platform for breast conserving surgery.

I.0.3 Contribution

The following chapters describe the development of an image guidance system that integrates supine MR images, optical tracking and digitization technology, patient specific biomechanical models for non-rigid registration, and tracked ultrasound for subsurface validation and performs initial validation on breast cancer patient data. Several contributions are presented in the following chapters. The work herein contains the first comprehensive description of system components involved in a surgical guidance system for breast cancer surgery. The extent of available data that can be incorporated into registration frameworks for image guided breast surgery is also reported. The use of intraoperative ultrasound to measure subsurface registration accuracy in the context of image guided breast surgery is also first reported here. Finally, preliminary studies on breast cancer patients under appropriate clinical conditions demonstrating system feasibility are presented.

CHAPTER II

Image to physical space registration of supine breast MRI for image guided breast surgery

II.1 Summary and Intent of Study

The intent of this chapter is to display the data collection techniques and system components for an image guidance system for breast cancer surgeries. The novel contribution of this study is the use of tracked intraoperative ultrasound digitized tumors to measure subsurface registration errors as well as the successful integration of system components to form the guidance system. The work in this chapter presents a preliminary study performed on one patient using only rigid registration to judge the feasibility of using supine magnetic resonance images to guide surgical procedures for breast cancer. This work was presented at the 2014 SPIE Medical Imaging Conference.

Appearing in:

R. H. Conley, I. M. Meszoely, T. S. Pheiffer, J. A. Weis, T. E. Yankeelov, and M. I. Miga, 'Image to physical space registration of supine breast MRI for image guided breast surgery', SPIE 2014 Medical Imaging: Image-guided Procedures, Robotic Interventions, and Modeling Conference, Vol. 9036, San Diego, CA, April 2014

II.2 Abstract

Breast conservation therapy (BCT) is a desirable option for many women diagnosed with early stage breast cancer and involves a lumpectomy followed by radiotherapy. However, approximately 50% of eligible women will elect for mastectomy over BCT despite equal survival benefit (provided margins of excised tissue are cancer free). Determining surgical margins intraoperatively is difficult and achieving negative margins is not as robust as it needs to be, resulting in high re-operation rates and often mastectomy. Magnetic resonance images (MRI) can provide detailed information about tumor margin extents, however diagnostic images are acquired in a fundamentally different patient presentation than that used in surgery. Therefore, the high quality diagnostic MRIs taken in the prone position with pendant breasts are not optimal for use in surgical planning/guidance due to the drastic shape change between preoperative images and the common supine surgical position. This work proposes to investigate the value of supine MRI in an effort to localize tumors intraoperatively using image-guidance. Mock intraoperative setups (realistic patient positioning in non-sterile environment) and preoperative imaging data were collected from a patient scheduled for a lumpectomy. The mock intraoperative data included a tracked laser range scan of the patient's breast surface, tracked center points of MR visible fiducials on the patient's breast, and tracked B-mode ultrasound images. The preoperative data included a supine MRI with visible fiducial markers. Fiducial markers localized in the MRI were rigidly registered to their mock intraoperative counterparts using an optically tracked stylus. The root mean square (RMS) fiducial registration error using the tracked markers was 7.5 mm. Following registration, the average closest point distance between the MR generated surface nodes and the LRS point cloud was 1.760.502 mm

II.3 Introduction

Due to mass breast cancer screenings, women are being diagnosed at earlier stages with smaller tumors. Therefore, breast conserving therapy (BCT) is a viable option for many women with early stage breast cancer, provided that negative margins (no cancer cells present on resected specimen) and acceptable cosmetic outcomes can be achieved. Breast conserving therapy involves a lumpectomy (removal of tumor with a margin of surrounding healthy tissue) followed by radiation therapy. For decades, BCT has shown to have the same survival rate as mastectomy (removal of the whole breast) (Fisher et al., 1977, 1989, 2002) in properly selected patients. However, there is an increasing trend toward choosing mastectomy over BCT due to surgical uncertainties (McGuire et al., 2009), despite recent research showing BCT to have improved disease-specific survival over mastectomy (Hwang et al., 2013).

The hesitation to choose BCT over mastectomy derives from the fact that determining surgical tumor margins intraoperatively is very difficult and negative margins are not always achieved, resulting in the need for

a second surgery or salvage mastectomy. Positive margins are often a result of an inability to visualize tumor location. Current techniques to localize breast lesions in the operating room include wire-guide localization and intraoperative ultrasound. Intraoperative ultrasound guidance is often ineffective for non-palpable breast tumors as approximately only half of these tumors can be visualized with ultrasonography (Klimberg, 2003). The standard technique for intraoperative tumor localization is wire-guided localization in which a radiologist inserts a wire into the tumor with guidance of ultrasound or mammography prior to entering the operating room. The surgeon then resects through the tissue being directed by the wire trajectory to the breast lesion. The shortcomings of this approach is that the guide wire does not provide a 3D perspective of the tumor and therefore cannot delineate tumor boundaries, which contributes to an unacceptable high rate of positive margins (Pleijhuis et al., 2009). In addition, often the trajectory of the wire is dictated by mammographic guidance and can at times represent an inefficient surgical route to the target which would direct the surgeon to navigate through excessive amounts of tissue, or would require the surgeon to make a visual estimation of a better route, both potentially leading to navigational errors.

Magnetic resonance (MR) imaging is the preferred imaging modality for preoperative clinical assessment and planning (Pleijhuis et al., 2009). However, preoperative planning images are acquired in the prone position with breast pendant, while surgery is performed in the supine position with arm extended. The breast undergoes significant deformation and shape change between the two positions. While prone breast MR images have superior image quality, they are not particularly valuable for surgical planning. Prone to supine image registration of breast MRI for aid in surgical planning has previously been proposed (Carter et al., 2008; Eiben et al., 2013; Behrenbruch et al., 2001; Carter et al., 2006b). Alternatively, in the work presented here, we propose to register supine MR images to physical space for intraoperative tumor localization. This approach has clear advantages: (1) the breast anatomy within the image volume is in a presentation that is representative of the operative setting, (2) tumor volume changes as it deforms under the breast's weight are captured better and should reflect better correlation between pathology reports and intraoperative observations, and (3) image-to-physical registration methods will be facilitated more readily.

Mock intraoperative data and preoperative data were collected from a patient scheduled for lumpectomy. The mock intraoperative data represents the localization of the patient's breast in physical space via multiple digitization methods (optically tracked laser range scan, stylus, and ultrasound imaging). Preoperative data includes MR images of the breast containing the lesion acquired in the supine orientation with MR-visible markers attached. Image to physical space registration was performed using landmarks visible in both the MR images and in physical space. The fiducial registration error (FRE), a measure of overall landmark misalignment, is reported as well as the closest point distance map of the registered preoperative and intraoperative surface. Subsurface registration accuracy was assessed by comparing the registered MR tumor contours to

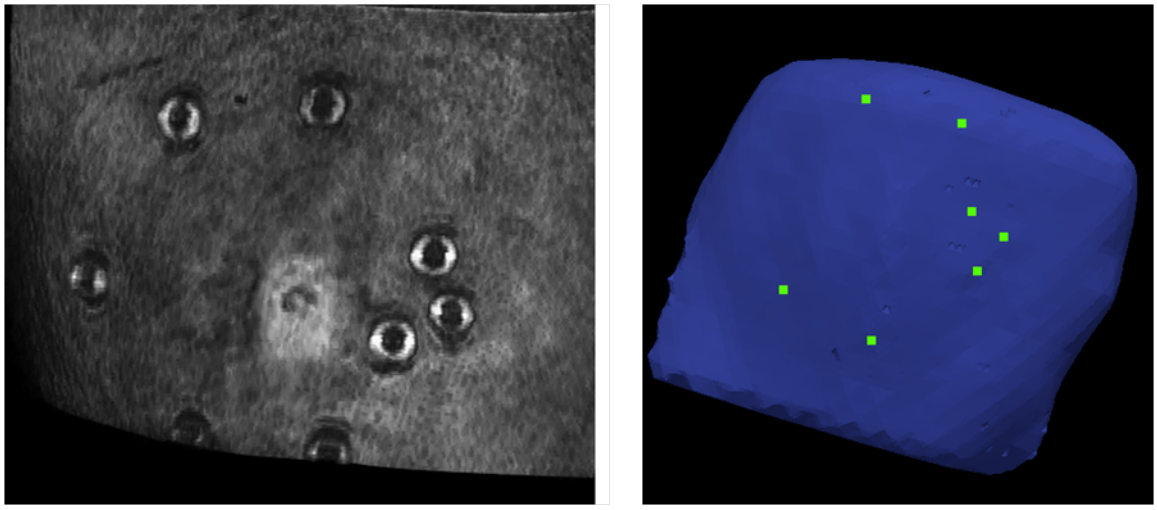

(a) (b)

Figure II.1: (a) Volume render of supine breast MRI. (b) Patient specific finite element mesh. Green points are manually selected fiducial centers.

their intraoperative counterparts as digitized by tracked ultrasound.

II.4 Methods

II.4.1 Preoperative data collection and patient specific modeling

In the imaging phase of the experiments, adhesive MR visible fiducial markers (IZI Medical Products, Owing Mills, MD) were distributed across the surface of the breast prior to imaging. The patient was placed in the supine position within a closed bore 3T Philips scanner. T1-weighted, 3D turbo field echo (TFE) with fat suppression images were acquired using a torso coil carefully placed as to not deform the breast surface. The acquired image volume was 512 x 512 x 160 mm^3 with a reconstructed voxel size of 0.391x0.391x1 mm^3. The breast and pectoral muscle were segmented using a semi-automatic active contour technique by ITK-SNAP's (Yushkevich et al., 2006) implementation of the Snakes (Kass et al., 1988) algorithm. The tumor was manually segmented and exported as a mesh from ITK-SNAP. A standard marching cubes algorithm (Lorensen and Cline, 1987) was used to create an isosurface of the breast and pectoral muscle and was further smoothed using FastRBF Toolbox (Farfield Technologies, Christchurch, New Zealand). From this surface, a tetrahedral mesh was generated using a custom mesh generator (Sullivan Jr et al., 1997). A volume render of the breast surface and the mesh generated by the MR volume is shown in Figure II.1. The green points in Figure II.1b indicate the centers of the markers and were manually determined using Analyze 9.0 (Mayo Clinic, Rochester, MN, USA).

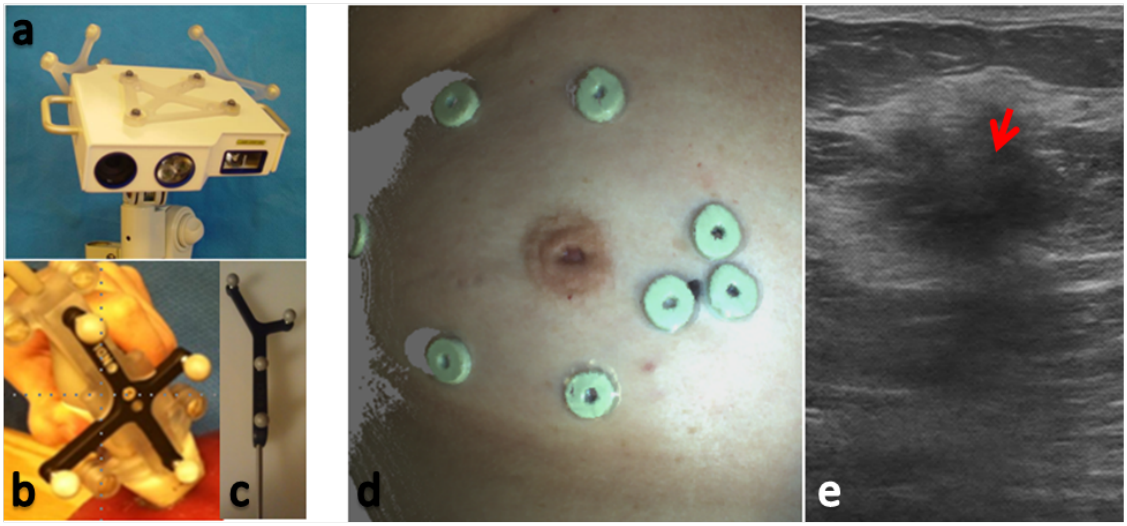

Figure II.2: (a) Laser range scanner with rigid bodies for tracking. (b) Ultrasound transducer with rigid body for tracking. (c) Tracked pen probe. (d) Textured point cloud produced by tracked laser range scanner with known 3D coordinates. The green rings are MR visible adhesive fiducial markers. (e) Example of a 2D ultrasound slice of a breast tumor (dark shadow shown by red arrow).

II.4.2 Mock intraoperative data collection

In our mock intraoperative setup, the patient was placed in a typical surgical orientation by a surgical oncologist to accurately depict operating room positioning. An optically tracked laser range scanner was used to scan the breast surface, providing a textured point cloud of the breast surface with known 3D coordinates. An optically tracked pen probe was used to collect the location of the centers of each of the fiducial markers. Finally, tracked ultrasound images were collected to provide the physical location of the tumor with respect to the breast surface. In this experiment, ultrasound images were acquired using the Acuson Antares system (Siemens Medical Solutions USA, inc, Mountain View, CA) using a VFX13-5 linear array probe with the a depth of 6 cm and frequency of 10 MHz. The ultrasound images were tracked in 3D by collecting synchronized video and tracking data on a host PC with the utilization of software based on the Visualization Toolkit (VTK). The ultrasound images were calibrated to physical space using a method (Muratore and Galloway Jr, 2001) based on the relationship between an optically tracked pointer and an optically tacked ultrasound transducer. Image to physical space registration between points located in the ultrasound image plane and their physical space counterparts determined by the tracked pen probe was performed to transform an ultrasound image into physical space. Following calibration, the compression of tissue caused by the ultrasound transducer was compensated for using a model based correction technique (Pheiffer et al., 2014).

II.4.3 Registration technique

MR-digitized marker locations were rigidly registered to the mock intraoperative tracked stylus points using a 3D point-based singular value decomposition registration algorithm (Sonka and Fitzpatrick, 2000), yielding a 4x4 transformation matrix. The fiducial registration error (FRE), a measure of overall landmark misalignment, is reported according to equation II.1.

$$FRE = \sqrt{\frac{1}{N}\sum_{i=1}^{N}(R(x_i + \Delta x_i)) + t - (y_i + \Delta y_i)} \tag{II.1}$$

where x_i and y_i are 3×1 vectors of corresponding points in two spaces, Δx_i and Δy_i are the fiducial localization errors for each point in the two spaces, N is the total number of fiducials, R is a 3×3 rotation matrix and t is a 3×1 vector containing displacements. With respect to surface fit assessment, the closest point distance map between the LRS point cloud and the MR generated mesh is reported.

II.4.4 Subsurface validation and ultrasound image processing

Compression of the breast tissue by the ultrasound transducer leads to incorrect measurements of tumor size and location. In this paper, we utilize a previously developed model based correction scheme developed by Phieffer et al (Pheiffer et al., 2014) to compensate for the compression of the target by the ultrasound transducer. The method utilizes the position of the tracked ultrasound probe to measure 3D displacements to drive a linear elastic correction model. The relative positions of the probe surface can be used to estimate the displacement of the breast tissue. Once a registration is made between the patient specific MR mesh and physical space, the ultrasound probe is now in the same space as the mesh. The probe surface will be located slightly below the surface of the mesh, depending on the compression of the tissue by the user. The pose of the probe surface provides Dirichlet boundary conditions for a forward linear elastic model that deforms the patient specific mesh to the compressed state exerted by the probe. The deformation field generated by this model is then applied in reverse manner to deform/correct the ultrasound slices and the segmented tumor contours such that they are correctly rendered in the uncompressed state associated with the pre-procedural supine MR orientation.

The subsurface tumor registration accuracy was measured by comparing the location of the tumor contour in the compression corrected ultrasound image and the tumor contour in the MR volume. The distance between the centroid of the US tumor and the MR tumor is reported. The modified Hausdorff distance (MHD) (Dubuisson and Jain, 1994) between the MR tumor contour and the US image contour is reported for seven ultrasound slices. The MHD is defined for two contours, A and B in accordance with equations II.2

and II.3.

$$d(A,B) = \frac{1}{N_a}\sum_{a\varepsilon A} min_{b\varepsilon B}(||a-b||) \tag{II.2}$$

$$MHD = max(d(A,B),d(B,A)); \tag{II.3}$$

The mean closest point distance d(A,B) is calculated in the direction from A to B, and then again from B to A. MHD is the maximum mean closest point between the two contours.

II.5 Results

The digitized breast surface acquired by the tracked laser range scanner was registered to the patient specific mesh using corresponding landmarks. The digitized breast surface is shown registered to the patient mesh in Figure 3a. The fiducial registration error was 7.4 mm. Figure II.3b shows the mesh and MR fiducial center points with the registered physical space fiducial centers. The surface alignment was inspected by calculating the signed closest point distances between the point cloud and mesh surface nodes. The average closest point distance was 1.76+/- 0.502 mm. A signed closest point distance map is shown in Figure II.3c. Figure II.3d shows how tumor location can be viewed in respect to the breast surface by superimposing the LRS point cloud with select ultrasound slices.

Following registration, the ultrasound slices and their corresponding tumor contours are corrected to compensate for the tissue compression applied by the ultrasound transducer. Figure II.4 shows an uncorrected and a corrected ultrasound slice. The blue outline is the ultrasound tumor contour while the red outline is the registered MR tumor contour. The average MHD value for the seven uncorrected US tumor contours was 2.68 +/- 0.6846 mm. The average MHD value for the seven corrected US tumor contours was 2.0814 +/- 0.4454 mm. The average distance from the centroid of the uncorrected US tumor contour and the MR tumor centroid was 3.93 +/- 1.2795 mm, while the centroid distance from the corrected US contours was 3.212 +/- 0.985 mm. Figure II.5 shows two plots, one of the MHD values for the corrected and uncorrected tumor contours and the centroid distances for the corrected and uncorrected tumor contours. In each case, the corrected ultrasound contours yielded a smaller average distance than the uncorrected ultrasound contours. Figure II.6 shows three out of the seven slices processed and show the corrected ultrasound slices overlaid onto their corresponding MR slices. The right hand column of Figure II.6 shows US (blue) and MR (red) tumor contours as well as the reported MHD value between the two contours.

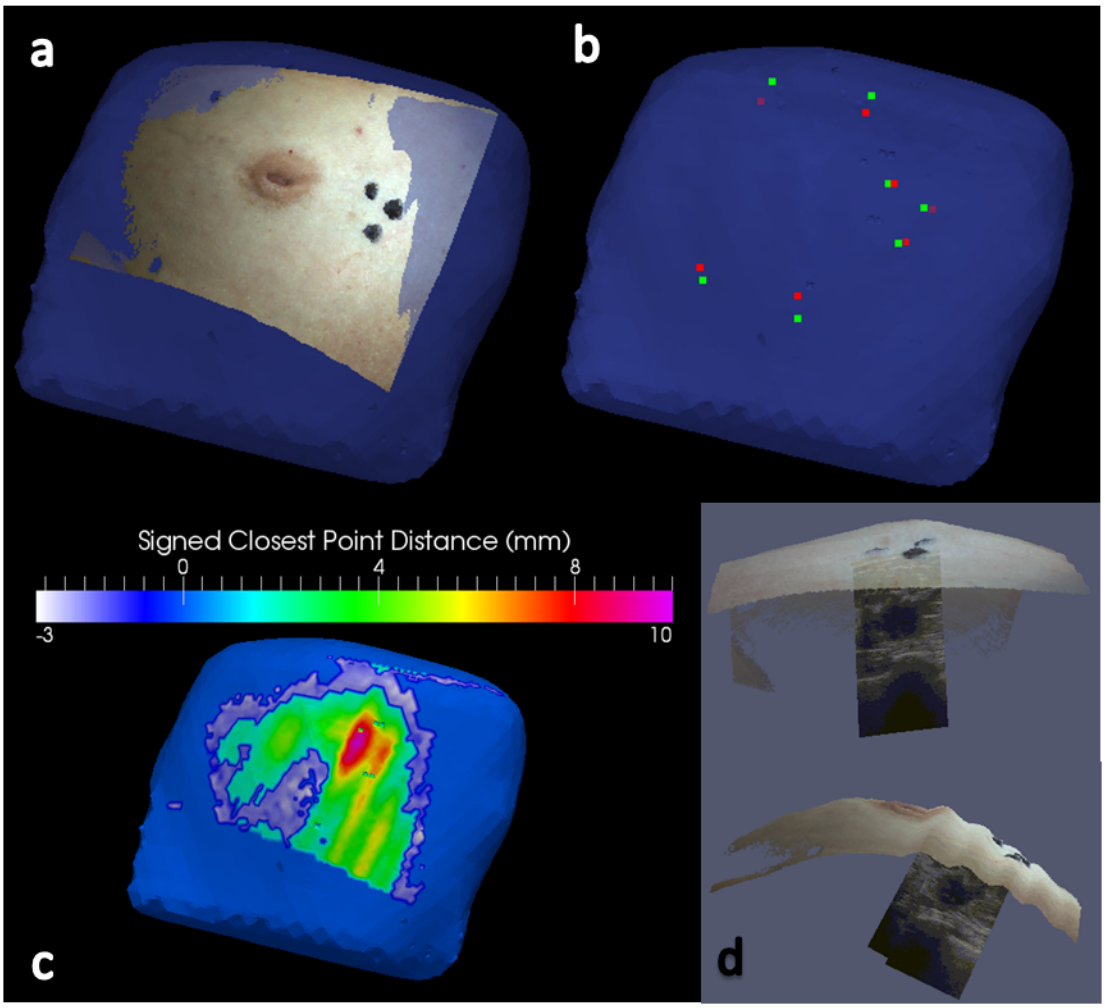

Figure II.3: (a) Registered digitized breast surface overlaid onto MR generated mesh. (b) MR fiducial center points (green) with registered physical space fiducial center points (red) overlaid onto patient specific mesh surface nodes. (d) Two orthogonal views of a textured point cloud of the breast with calibrated ultrasound slices showing tumor location in physical space.

II.6 Discussion

The results of the overall surface alignment are on average less than 2 mm. However, multiple inspiration and expiration events happen over the 20-40 seconds that it takes for the laser range scanner to pass across the whole surface of the breast. This causes a rippling effect to be present in the point cloud collected by the LRS. This is evident in the bottom image in Fig. II.3d. The rippling due to respiratory motion increases a mismatch between the point cloud and mesh surface. This is propagated to the closest point distance map shown in Fig. II.3c where the largest error (10 mm) is at the location of the largest inspiration peak on the point cloud. These respiratory affects can be diminished by using a faster scanner or a different digitization device, such as a stereo vision camera system, where capture of the breast surface occurs at the speed of the

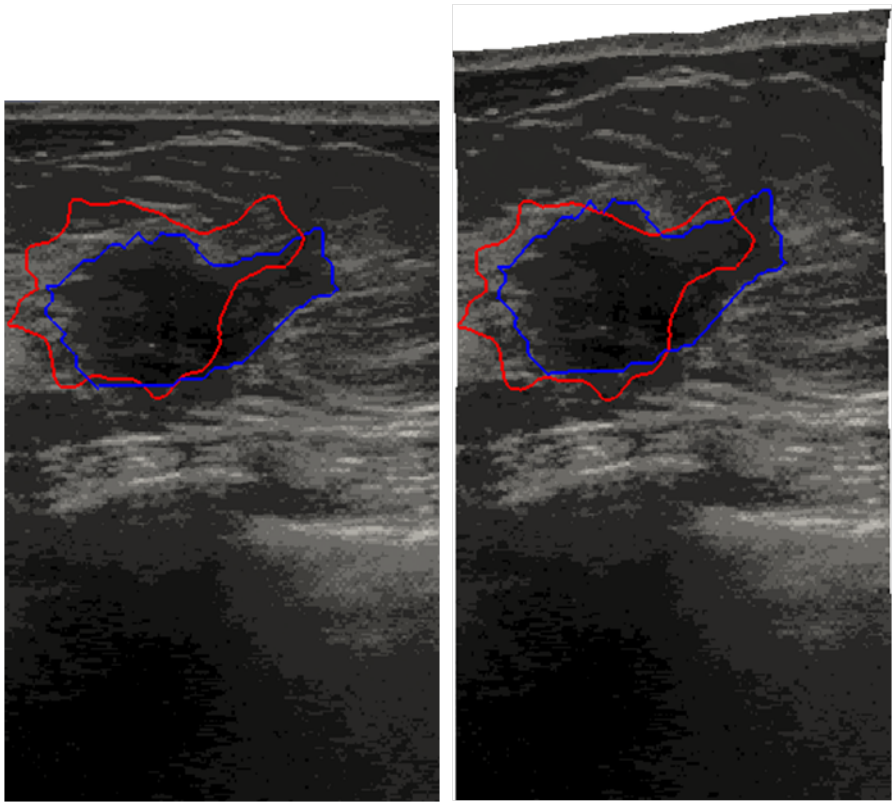

Figure II.4: Left: Uncorrected ultrasound slice with uncorrected ultrasound tumor contour (blue) and MR contour (red). Right: corrected ultrasound slice with ultrasound tumor contour (blue) and MR contour (red).

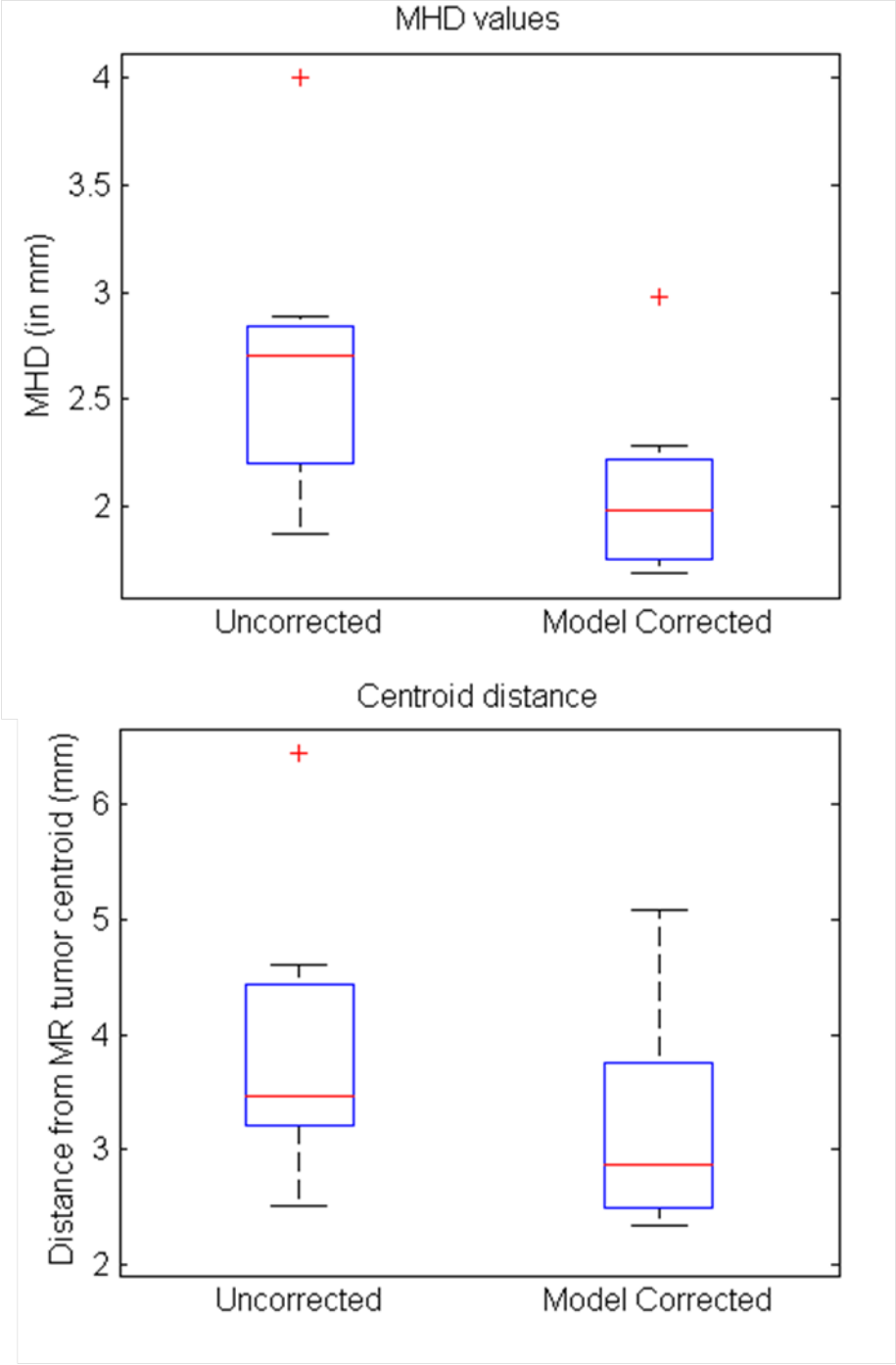

Figure II.5: Tumor alignment errors for the corrected and uncorrected ultrasound slices. The modified hausdorff distance (MHD) between the co-aligned MR tumor contours and the US tumor contours are reported for the uncorrected and model corrected ultrasound slices. The distance between the MR tumor centroid and the US tumor centroids are also reported. The red line inside the box represent the mean and the edge of the boxes represent the 25th and 75th percentiles, and the lines extend to the most extreme observation points not considered as outliers.

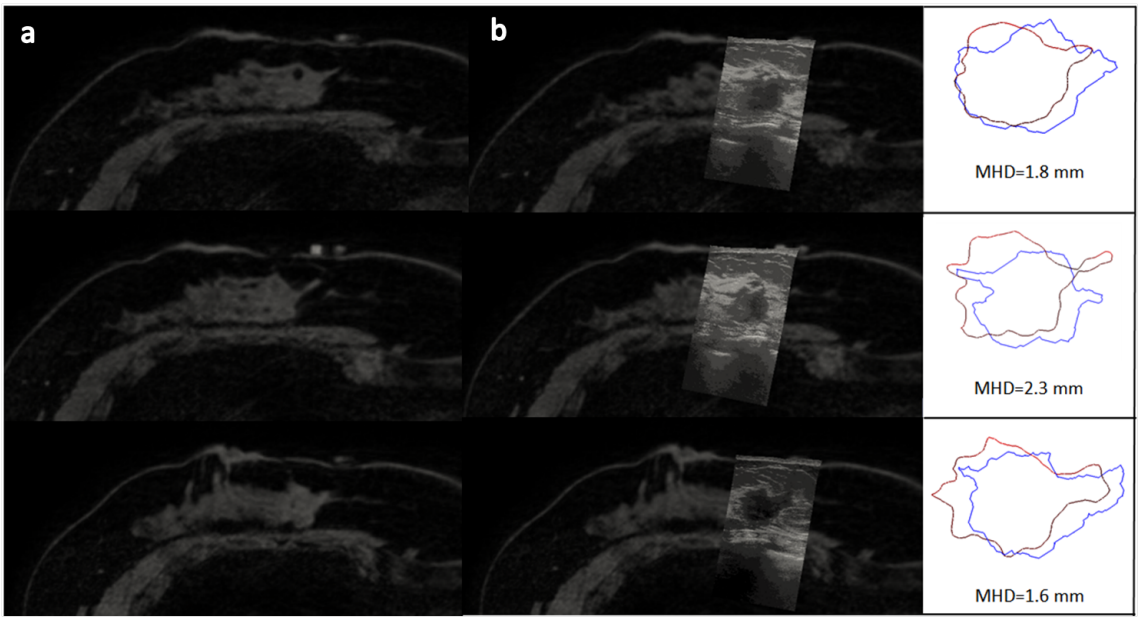

Figure II.6: column (a) is three supine MR slices, Column (b) shows three different registered ultrasound slices overlaid on the corresponding MR slice. The third column shows MR contours (red) and corrected US contours (blue) as well as the MHD values for the two contours.

camera frame rate (usually $<$1second).

The model corrected ultrasound slices produced a better average alignment with the MR tumor contours than the uncorrected tumor contours. A Wilcoxon signed rank test was performed to test for differences between the corrected and uncorrected MHD values (significance at p-value < 0.05). There was a significant improvement in tumor alignment when using the model corrected ultrasound slices (p=0.015). There was not a significant difference (p-value=0.078) between the corrected and uncorrected tumor centroid distances, although a trend was identified with lower errors associated with corrected tumor contours. More study is needed to provide a statistically significant result. Sources of variability that may have contributed to the error is the uncertainty of manual segmentation of the tumor borders in the ultrasound and MR images. Ideally, in the future we will acquire pre and post contrast enhanced magnetic resonance images to get a concrete and user independent tumor border in the MR images. It should also be noted that multiple sources of error may have contributed to the final misalignment of the US and MR tumor contours. Errors associated with the optical tracking equipment, tracked ultrasound calibration, and ability to accurately localize the fiducial center points may be related and not necessarily additive leading to an uncertainty of how the noises of the system propagate. This uncertainty is characteristic of any realistic guidance platform.

While we are pleased that the surface of the LRS and the surface of the patient mesh were adequately aligned, our real concern is the accuracy of the subsurface features, particularly the cancerous lesion located

within the fibro glandular tissue. Fig. II.6 shows successful alignment between the ultrasound images to the MR slices, with especially promising correspondence between the pectoral muscle and fibroglandular tissue in the MR and US images. The average MHD and centroid distance values of the model corrected ultrasound slices and the MR tumors were around 2-3 mm. A surgical oncologist typically aims to remove 5mm of surrounding healthy tissue, so a 2-3 mm error is acceptable for this surgical domain.

II.7 Conclusion

In this work we present a workflow for the acquisition of data, processing of images, creation of patient specific models, and validation for an image based guidance system for the removal of cancerous breast lesions. We collected preoperative images and mock intraoperative data from a breast cancer patient scheduled for a lumpectomy to survey our ability to register and validate our alignment accuracy. With our subsurface alignment errors being on average less than 5 mm, we are encouraged to further investigate the potential of utilizing the combination of supine magnetic resonance images, patient specific biomechanical models, and intraoperative tracked ultrasound as a framework for an image guidance system for breast conservation surgeries.

CHAPTER III

Realization of a biomechanical model assisted image guidance system for breast cancer surgery using supine MRI

III.1 Summary and Intent of Study

This chapter builds upon the work completed in Chapter II. Here we present two patient subjects as an initial investigation towards the realization of a biomechanical model assisted surgical platform. This chapter employs the use of a novel biomechanical model based nonrigid registration to correct preoperative patient specific models and images to better match the surgical presentation of the breast. The model presented in this chapter was purposefully designed to be work-flow friendly and establish a baseline understanding of the capability of a model-based correction technique. The significance of this work is that it is the first full description and implementation of a comprehensive system for image guided resection of breast tumors. This work is the first to incorporate the chest wall as a rigid feature to improve alignment. While still preliminary, the results are very encouraging at this early stage and several avenues for future work exist. This work has been accepted for oral presentation at the International Conference on Information Processing and Computer-Assisted Interventions (IPCAI) 2015 conference. The work has also been submitted to the International Journal of Computer Assisted Radiology and Surgery (IJCARS).

Appearing in:

Conley RH, Meszoely IM, Weis JA, Pheiffer TS, Arlinghaus LR, Yankeelov TE, and Miga MI. ”Realization of a biomechanical model assisted image guidance system for breast cancer surgery using supine MRI”, In: Information Processing in Computer Assisted Interventions. Lecture Notes in Computer Science. Springer International Publishing, 2015

III.2 Abstract

Purpose: Unfortunately, the current re-excision rates for breast conserving surgeries due to positive margins average 20-40%. The high re-excision rates arise from difficulty in localizing tumor boundaries intraoperatively and lack of real time information on the presence of residual disease. The work presented here introduces the use of supine magnetic resonance (MR) images, digitization technology, and biomechanical models to investigate the capability of using an image guidance system to localize tumors intraoperatively.

Methods: Preoperative supine MR images were used to create patient specific biomechanical models of the breast tissue, chest wall, and tumor. In a mock intraoperative setup, a laser range scanner was used to digitize the breast surface and tracked ultrasound was used to digitize the chest wall and tumor. Rigid registration combined with a novel nonrigid registration routine was used to align the preoperative and intraoperative patient breast and tumor. The registration framework is driven by breast surface data (laser range scan of visible surface), ultrasound chest wall surface, and MR-visible fiducials. Tumor localizations by tracked ultrasound were *only* used to evaluate the fidelity of aligning preoperative MR tumor contours to physical patient space. The use of tracked ultrasound to digitize subsurface features to constrain our nonrigid registration approach and to assess the fidelity of our framework makes this work unique. Two patient subjects were analyzed as a preliminary investigation towards the realization of this supine image guided approach.

Results: An initial rigid registration was performed using adhesive MR-visible fiducial markers for two patients scheduled for a lumpectomy. For patient 1, the rigid registration resulted in a root mean square fiducial registration error (FRE) of 7.5 mm and the difference between the intraoperative tumor centroid as visualized with tracked ultrasound imaging and the registered preoperative MR counterpart was 6.5 mm. Nonrigid correction resulted in a decrease in FRE to 2.9 mm and tumor centroid difference to 5.5 mm. For patient 2, rigid registration resulted in a FRE of 8.8 mm and a 3D tumor centroid difference of 12.5 mm. Following nonrigid correction for patient 2, the FRE was reduced to 7.4 mm and the 3D tumor centroid difference was reduced to 5.3 mm.

Conclusion: Using our prototype image guided surgery platform, we were able to align intraoperative data with preoperative patient specific models with clinically relevant accuracy; i.e., tumor centroid localizations of approximately 5.3 -5.5 mm.

III.3 Introduction

Breast cancer is the most frequently diagnosed cancer in women and is also the leading cause of cancer related deaths among women worldwide, with 1.7 million new cases being diagnosed and more than 500,000 deaths occurring in 2012 (Jemal et al., 2011). Breast cancer treatment is dependent upon multimodal therapy with surgery being a primary component, especially for early stage cancers. Mastectomy (total removal

(a) Prone MR image of breast (b) OR presentation (c) supine MR image of breast

Figure III.1: Demonstration of the challenge of using preoperative images for surgical guidance. (a) and (c) are axial slices of T_1-weighted THRIVE sequence MR images in the prone and supine positions with red ovals designating the same tumor in the same axial slice. Changes in patient setup cause the tumor to move, yielding the diagnostic scan in (a) less valuable for locating the tumor in the surgical setup, shown in (b).

of the breast) was the most common procedure choice for newly diagnosed breast cancer patients until the 1980s when studies revealed that lumpectomy, the far less disfiguring option, was shown to have the same 10 year survival rate as mastectomy (Fisher et al., 1985). Despite this fact, approximately 25-50% of patients eligible for breast conservation therapy (BCT) will choose mastectomy over lumpectomy (Fancher et al., 2009; Adkisson et al., 2012). A substantial concern of BCT patients is whether or not negative margins will be obtained in the initial surgery. Negative margins are achieved when no cancer cells are present on or near (usually within 5-10 mm) the border of the excised tissue and are considered necessary for a successful lumpectomy. Unfortunately, the current re-excision rates due to positive margins average 20-40% (Landercasper et al., 2014). Failure to achieve negative margins can result in the delay of radiation treatment, increase risk for local recurrence, cause psychological and physical stress on the patient, compromise cosmetic results, and increase cost.

The high re-excision rates arise from the difficulty in localizing tumor boundaries intraoperatively and lack of real time information on the presence of residual disease (Pleijhuis et al., 2009). The challenge in determining surgical margins intraoperatively is that geometric and spatial cues are quickly lost in the surgical presentation. Equally confounding is that valuable diagnostic images are acquired in a significantly different breast presentation than the typical surgical setup. Diagnostic and biopsy information are driven by mammography and preoperative MR images in which the patient is standing or lying prone with pendant breasts, while surgical presentation is in the supine position. An example of this challenge is displayed in Fig. III.1, where the breast undergoes significant shape change between the prone and supine positions causing the tumor to deform and change location.

Current localization strategies used in the operating room (OR) include intraoperative ultrasound, wire

guided approaches, and radio-guided occult lesion localization. Prospective studies report that wire guide localization results in positive margins in 38-43% of patients undergoing BCT (Allweis et al., 2008; Tafra et al., 2006). Intraoperative ultrasound (iUS) has been shown to improve BCT (Davis et al., 2011). However, iUS is limited by the fact that only 50% of non-palpable tumors are visible by ultrasound in the breast (Pleijhuis et al., 2009). The shortcomings of radio-guided occult lesion localization is that the radioisotope must be accurately placed into the tumor and diffusion of the radiotracer into surrounding tissue decreases accuracy of the tumor location (Pleijhuis et al., 2009).

Due to the current limitations of intraoperative tumor localization approaches, the efficacy of using MR data alignment strategies has been investigated but challenges in surgical presentation have been identified. There is little doubt that the use of MR data to influence surgical planning has important implications in the surgical management of patients (Braun et al., 2008; Buxant et al., 2007). We believe that better image-to-physical data alignment strategies can be used more directly for better surgical management. To achieve this, methods using biomechanical models for prone-to-supine registration of MR images have been suggested (Carter et al., 2008; Han et al., 2014a) . Recently, utilization of supine MR images for surgical guidance have been considered in frameworks for image guided breast surgery (Siegler et al., 2011; Alderliesten et al., 2010; Conley et al., 2014). Alignment of pre-surgical supine MR images to surgically oriented MR images using surface markers has also been shown to be feasible (Ebrahimi et al., 2014). Preoperative supine MR images registered using surface markers coupled with an intraoperative optical scan of the breast has also demonstrated qualitative alignment value (Pallone et al., 2014). While encouraging, the integration of supine MR images, optical tracking and digitization technology, patient specific biomechanical models for nonrigid registration, and tracked ultrasound for subsurface feature localization has yet to be realized as a surgical guidance platform for breast conserving surgery. This paper integrates these components and reports preliminary experiences with this surgical platform in two patient cases. In addition, subsurface target accuracy is assessed independently using tracked ultrasound imaging of echogenic tumors in both cases.

III.4 Methods

Two breast cancer patients scheduled for surgery were selected in a Vanderbilt IRB approved bystander study to evaluate the feasibility and accuracy of our image guidance platform. In Fig.III.2, a schematic overview demonstrates the structure of the proposed system with required data inputs and generalized outputs at each step. Both subjects had ultrasound visible tumors. While our guidance platform does not require ultrasound visible tumors, their echogenic visibility in this study was particularly useful for evaluating the subsurface alignment accuracy of our registration approach.

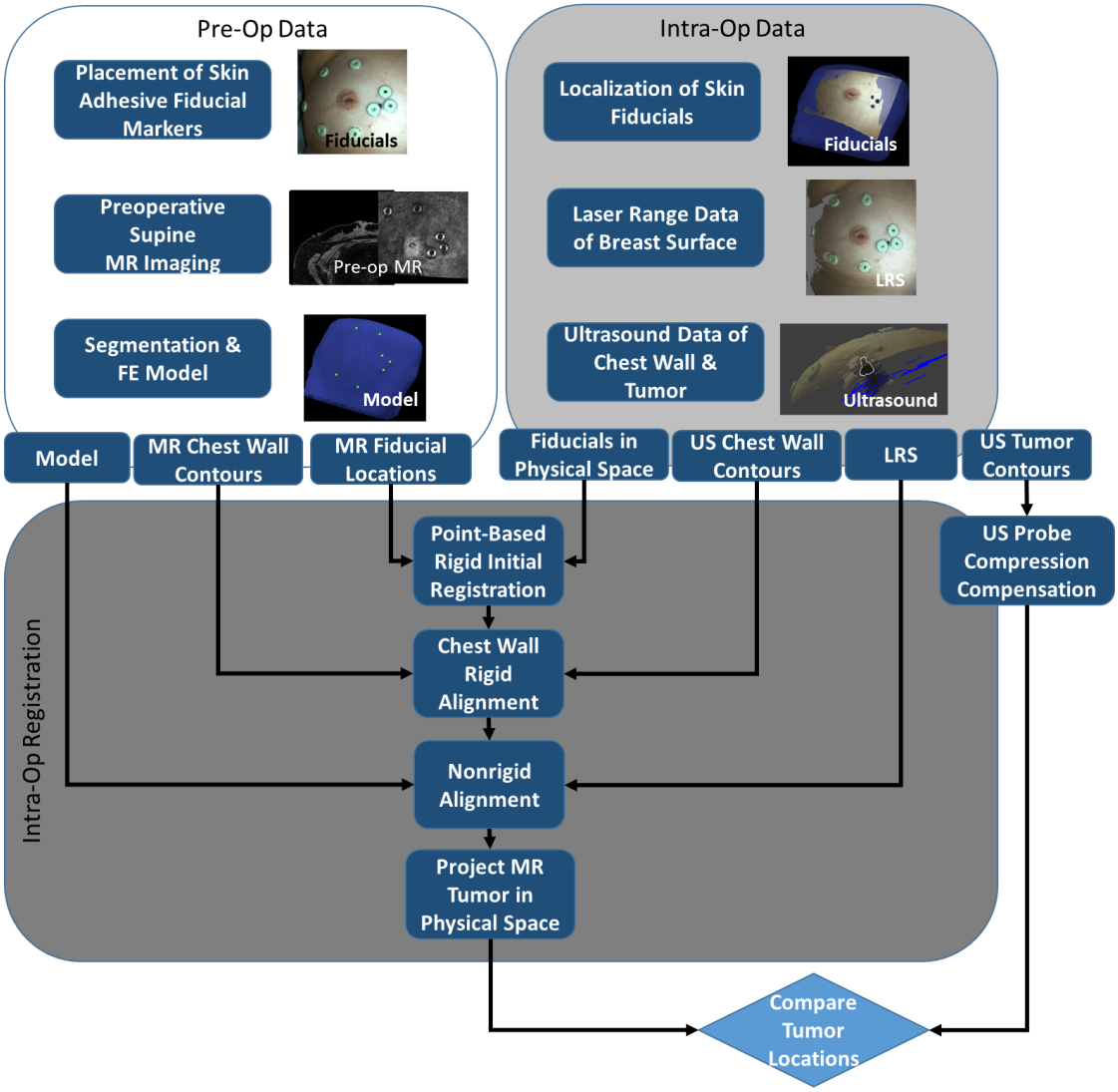

Figure III.2: Overview of surgical guidance platform and validation framework. The preoperative (preOp) and intraoperative (intraOp) data panels summarize the important information gathered at each step. This information is then systematically incorporated into an intraOP registration framework. The final outcome is a preoperative tumor mapped to physical space which can then be quantitatively compared to the location of the tumor in the OR.

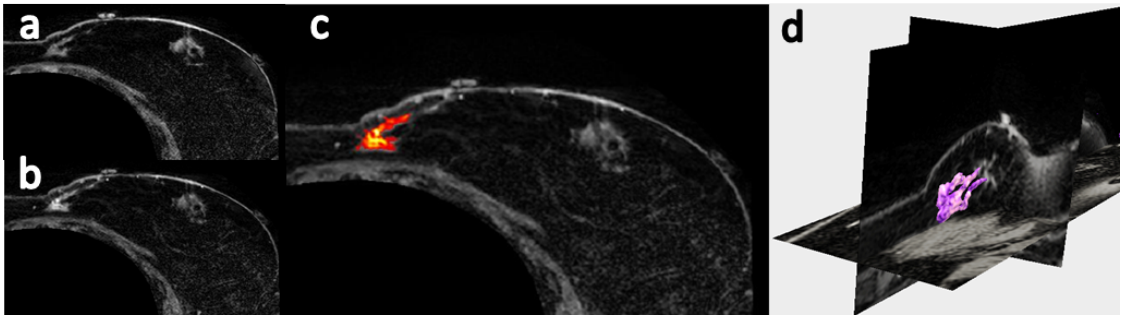

Figure III.3: Axial slices of supine MRI of patient volunteer with (a) pre-contrast, (b) post-contrast injection,(c) contrast-enhanced image with colored overlay showing tumor, and (d) 3D segmentation of tumor (magenta).

III.4.1 Preoperative Data Collection

III.4.1.1 Supine MR Imaging

Preoperative supine MR images were acquired for each patient and were used to create patient specific biomechanical models of the breast tissue, chest wall, and tumor. MR visible adhesive skin fiducial markers (IZI Medical Products, Owing Mills, MD) were placed over ink markings distributed across the breast surface. The patient was carefully positioned in a closed bore 3T Achieva MR scanner (Philips Healthcare, Best, The Netherlands). A 16-channel sensitivity encoding (SENSE) torso coil was situated carefully as to not deform the breast, and the ipsilateral arm was placed above the patient's head to more closely replicate surgical presentation. High resolution anatomical images were acquired with a T_1-weighted, 3D turbo field echo sequence with fat suppression, a field of view of $200\times200\times160$ mm^3, and a reconstructed voxel size of $0.391\times0.391\times1$ mm^3. Recently, we have achieved successful acquisitions of contrast enhanced supine images, an example of a contrast enhanced image volume of a patient volunteer is shown in Fig. III.3. For the patient subjects studied herein, tumors were identified from the diagnostic MR supine images and were segmented semi-automatically.

III.4.1.2 Patient Specific Model

The supine image volume from each patient was segmented into breast tissue, tumor, and chest wall (pectoral muscle) using a semi-automatic segmentation technique by Insight Registration and Segmentation Toolkit (ITK)-SNAP (Yushkevich et al., 2006). Fig. III.4a illustrates the segmentation step for patient 1. The locations of the synthetic fiducial center points were manually determined and recorded (Fig. III.4b). Following segmentation, a binary mask of the whole breast was used to generate an isosurface using a standard marching cubes algorithm (Lorensen and Cline, 1987). The isosurface was then smoothed with a radial basis function using FastRBF Toolbox (Farfield Technologies, Christchurch, New England). From this surface, a finite el-

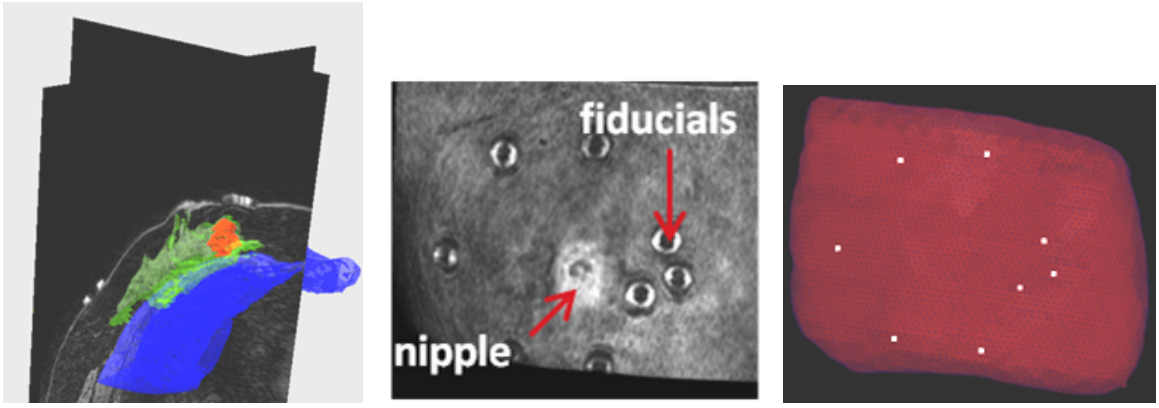

(a) (b) (c)

Figure III.4: Segmentation of preoperative supine MR images: (a) segmentation of glandular tissue in green, chest wall in blue, and tumor in red. (b) is a volume render of the supine MR image, (c) preoperative mesh showing location of fiducial centers in white.

ement tetrahedral mesh was generated using a custom mesh generator (Sullivan Jr et al., 1997) with a mesh edge-length resolution of approximately 3 mm (Fig. III.4c).

III.4.2 Mock Intraoperative Data Collection

As an initial investigation, a mock intraoperative setup to collect simulated intraoperative data was performed for each patient. In this study, mock intraoperative data was collected to avoid workflow disruptions in the OR and was performed on the same day as preoperative imaging to minimize patient volunteer time. The true intraoperative scenario would involve intraoperative data, such as that shown in Fig. III.5, to be collected during surgery. To address realistic patient conditions in the mock setup, positioning was performed by a surgical oncologist, to accurately depict OR positioning. Once complete, skin fiducials are digitized with an optical stylus, a laser range data is acquired, and an ultrasound examination is performed. In the following subsections, the extent of this data and its integration is explained.

III.4.2.1 Surface and Feature Digitization

A custom-built, optically tracked laser range scanner (Pathfinder Technologies, Inc, Nashville, TN, USA) was used to digitize the breast surface by sweeping a laser line over the breast surface and recording geometric points along with color information of the visible field (Fig. III.5a top, Fig. III.5b), yielding a textured point cloud with known 3D coordinates in physical space. The physical space points corresponding to the MR visible fiducial center points are determined by the black ink markings that were placed on the patient's skin prior to adhering the MR visible fiducials. An optically tracked stylus was used to collect the location of the ink markings. The textured point cloud was used to confirm the location of the fiducial points by comparing

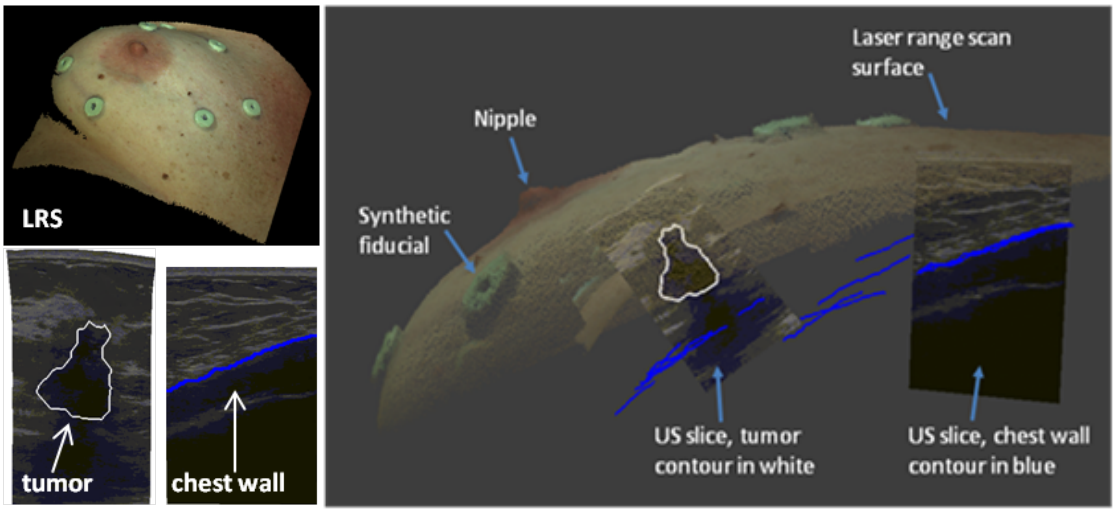

(a) (b)

Figure III.5: (a) Top: LRS scan of patient 2 breast. Bottom left: compression corrected ultrasound image with tumor contour in white. Bottom right: ultrasound image with chest wall contour in blue. (b) Fusion display of tracked intraoperative data containing a textured point cloud, adhesive fiducial markers, tracked ultrasound images, tumor contour (white), and chest wall contours (blue).

the coordinates collected by the tracked stylus with the field of view color texture information collected from the laser range scanner. All geometric measurements were made with a Polaris Spectra (Northern Digital, Waterloo, ON, Canada) optical tracking system.

III.4.2.2 Ultrasound Exam

The ultrasound portion of this study was performed in two parts: (1) target B-mode imaging of tumor and (2) chest wall swabbing. Fig. III.5a bottom left and Fig. III.5a bottom right show representative contours of each, respectively. Ultrasound images were acquired using an Acuson Antares ultrasound machine (Siemens, Munich, Germany) using a VFX13-5 linear array probe set at 10 MHz. The depth was set at 6 cm to maintain visibility of the chest wall throughout the exam. A passive optically tracked rigid body was attached to the ultrasound transducer. The tracked ultrasound was calibrated using the method developed by Muratore et al. (Muratore and Galloway Jr, 2001) that takes multiple b-mode ultrasound images of a tracked stylus tip in the imaging plane to develop a rigid transformation between the image plane and physical space. Once calibrated, all pixels in the ultrasound plane have a corresponding 3D coordinate in physical space.

In addition to optical tracking for determining the location of ultrasound visualized structures, it is also important to correct the localization data of structures that are affected by ultrasound probe compression, namely the tumor (chest wall was assumed rigid). More specifically, since preoperative supine MR images

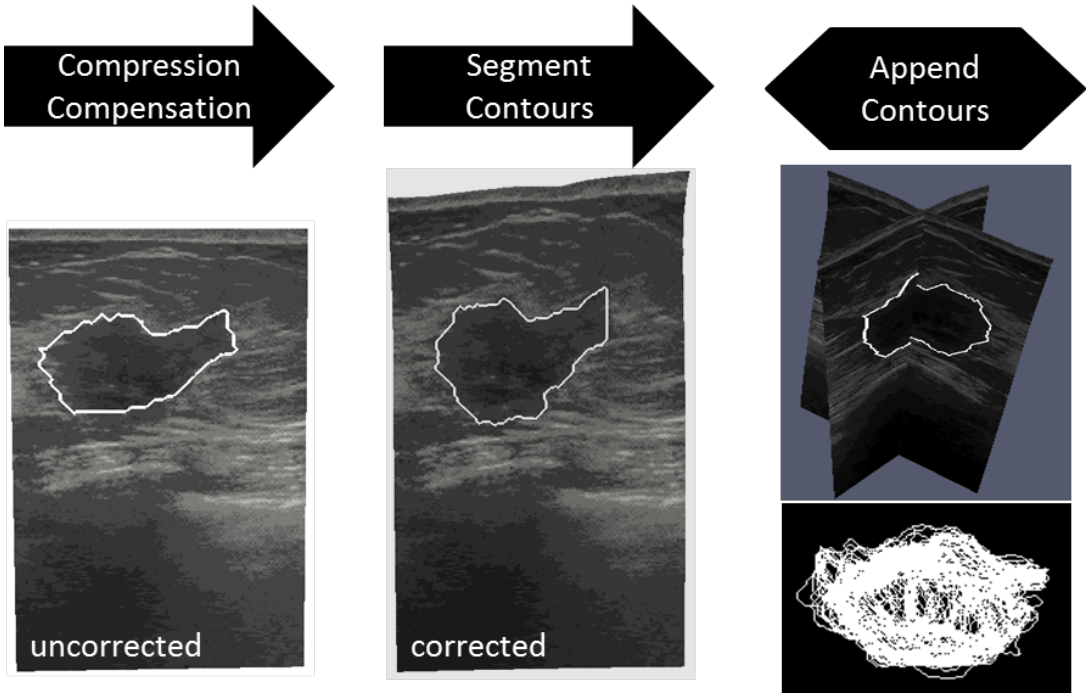

Figure III.6: Steps involved in processing tracked intraoperative ultrasound data. The ultrasound images are first corrected for tissue compression exerted by the ultrasound transducer. The tumor contour is then segmented in each 2D slice. Lastly, all contours are appended to form a 3D representation of the intraoperative tumor.

are acquired without this compression, a correction scheme to account for deformation induced by the probe itself is needed in all ultrasound images of the echogenic tumor. Reported in (Pheiffer et al., 2014), the fidelity of the method we utilized demonstrated reduced subsurface localization errors due to ultrasound probe compression by 67.8% and 51.6% in phantom and clinical experiments respectively. For the work reported in this study, it was particularly important to utilize these methods as tumor localization was serving as the primary means for accuracy evaluation of our platform.

Fig. III.6 provides a visual overview of the processing steps involved in acquiring tracked ultrasound data of the intraoperative tumor volume. Tumor borders are semi-automatically segmented using a custom implementation of the Livewire technique (Mortensen and Barrett, 1995). The acquired tumor ultrasound image/-contour is then corrected for probe deformation and each is appended, yielding a 3D point cloud set. Similar steps are performed for the chest wall but probe deformation compensation is not necessary. Fig. III.5b shows a comprehensive representation of all digitization data rendered consistently within physical space; textured point cloud, synthetic fiducial landmarks, and tracked ultrasound images of both probe-corrected tumor and chest wall ultrasound slices with segmented contours.

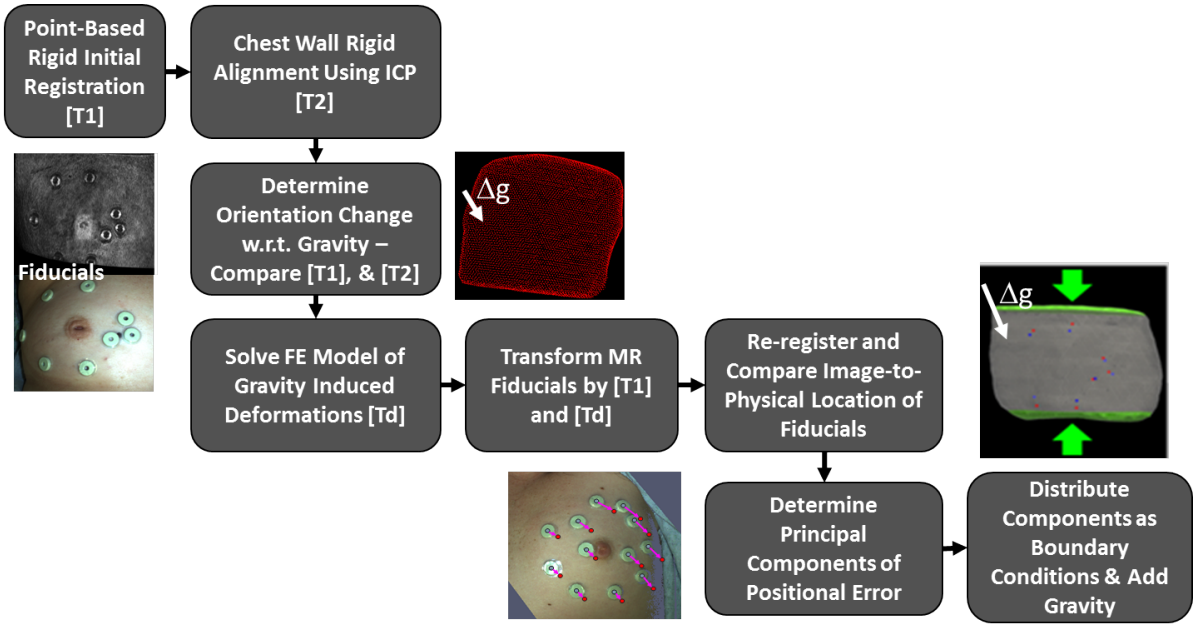

Figure III.7: Overview of the registration process beginning with rigid initialization and concluding with full nonrigid model compensation.

III.4.3 Registration Method

The entirety of our registration approach is captured in Fig. III.7. Briefly described, an initial rigid alignment is performed using the synthetic fiducials adhered to the breast. Once complete, a series of steps is conducted to estimate the influence of gravity-induced and ipsilateral arm position changes between supine imaging and surgical configurations. The influence of these variables is realized as a gravitational inducing body force and boundary conditions which are applied to a biomechanical model of the breast. Once complete, the combined rigid and nonrigid transformation provides a means to map preoperative tumor locations into physical space which can then be subsequently compared with a separate independent ultrasound identified tumor localization.

III.4.3.1 Rigid Alignment

An initial rigid alignment was performed by registering the MR-digitized marker locations to their intraoperative counterparts using a traditional 3D point based singular value decomposition registration algorithm (Sonka and Fitzpatrick, 2000). The point based registration algorithm finds the optimal translation and rotation to minimize the fiducial registration error (FRE) as defined by:

$$FRE = \sqrt{\frac{1}{N}\sum_{i=1}^{N}(R(x_i+\Delta x_i))+t-(y_i+\Delta y_i)} \tag{III.1}$$

where x_i and y_i are 3×1 vectors of corresponding points in two spaces, Δx_i and Δy_i are the fiducial localization errors for each point in the two spaces, N is the total number of fiducials, R is a 3×3 rotation matrix and t is a 3×1 vector containing displacements. The resulting translation vector and rotation matrix are applied to the preoperative data to provide an initial alignment with the intraoperative space.

III.4.3.2 Quantification of Gravity-induced Deformations

Based on initial studies investigating the use of point-based registration of skin fiducials, it was found that significant rotation of the breast occurs relative to the chest wall between supine imaging and intraoperative presentation in some cases. This results in a body force based deformation whereby the breast becomes free to move under the influence of gravity. To estimate this change, we have elected a novel strategy. The chest wall is designated from the preoperative supine images during our breast model building process (Section III.4.1.2). In addition, chest wall contours are also identified and segmented from our tracked ultrasound examination (Section III.4.2.2). Using the fiducial-based registration (Section III.4.3.1) as an initial configuration, a traditional iterative closest point (ICP) registration (Besl and McKay, 1992) was employed between the transformed preoperative chest wall points and the intraoperative chest wall contours as digitized by tracked iUS. The rotation matrix resulting from the ICP registration is applied to the intraoperative gravity vector (assumed to be in the direction normal to the patient's bed). Details of this approach are outlined in Algorithm 1.

Algorithm 1 Algorithm for finding gravity-induced deformations using ICP registration

1. Initialize by transforming preoperative chest wall contours to intraoperative space using transformation from III.4.3.1
2. Perform an ICP registration between MR chest-wall surface and iUS chest wall contours
3. Extract the rotation matrix from the final transformation and apply to the gravity vector in intraoperative space

$$\Delta g = R * g_{intraop} \tag{III.2}$$

where $g_{intraop}$ is a 3×1 vector containing the unit direction normal to the patient bed in intraoperative space

III.4.3.3 Mechanics-based Nonrigid Correction

Deformations due to gravity-induced changes derived from Algorithm 1 and tissue migration of the breast due to ipsilateral arm movement are estimated using a 3D linear elastic model. The model employs the

Navier-Cauchy equations and generates a displacement field for correction and is shown here:

$$\nabla \cdot (G\nabla u) + \nabla(\frac{G}{1-2\nu}(\nabla \cdot u)) + \rho(\Delta g) = 0 \tag{III.3}$$

where υ is Poisson's ratio, G is the shear modulus of elasticity ($G = E \ / \ 2(1+\nu)$), u is the 3D displacement vector, ρ is the tissue density, and Δg is the change in gravitational acceleration constant with respect to imaging and surgical presentations. Equation III.3 was solved using the Galerkin Method of Weighted Residuals with linear Lagrange polynomials defined locally on the tetrahedral elements as the supporting basis and weighting functions. Solving this system results in displacement vectors defined at each node that satisfy static equilibrium conditions. The displacements are then applied to deform the preoperative mesh. In this work, an elastic modulus (E) of 1 kPa, tissue density of 1000 kg/m^3, and Poisson's ratio of 0.485 were applied for the whole breast volume.

III.4.3.4 1st Model Solve- Application of Gravity-induced Deformations

Gravity induced deformations were simulated by supplying the elastic model with a body force of tissue weight based on the change in acting gravity direction as determined in Section III.4.3.2. We again assume that the chest wall is a rigid fixed structure. Therefore, the boundary conditions applied to this model solve imposed fixed chest wall nodes (zero displacement) with stress-free boundary conditions elsewhere. The displacements generated from this model solve were applied to the preoperative mesh and used to estimate the remaining positional error of fiducial targets.

III.4.3.5 Final Model Solve

Nonrigid deformations of the breast due to ipsilateral arm movement were accounted for by applying Dirichlet boundary conditions at control surfaces along the inferior-superior surfaces of the model mesh based on preoperative imaging data. The nodes corresponding to the interior chest wall and the medial breast surface were fixed. The medial breast face was fixed because negligible movement occurs in the vicinity of the patient's sternum. The remainder of the breast surface; i.e., the visible breast during presentation, was designated as stress free.

The locations, direction and magnitude of the applied Dirichlet boundary conditions for the inferior-superior surfaces were determined by analyzing the misalignment between the co-registered surface fiducials after gravity-induced changes were taken into account. In both patient cases, a reduced stretching of the breast between preoperative and intraoperative states was observed and used to determine model displacement boundary conditions at the inferior-superior surfaces. This reduced stretching phenomenon is shown in

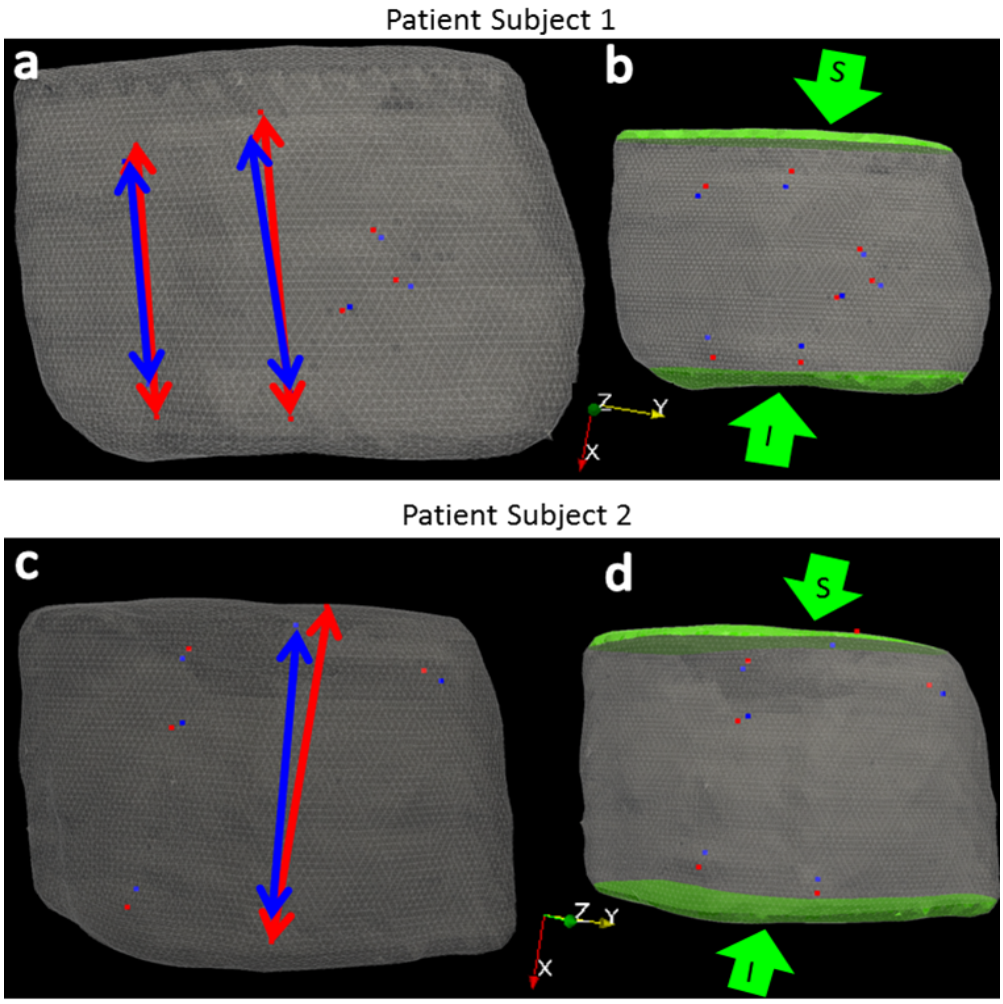

Figure III.8: (a,c) preoperative mesh with arrows showing preoperative (red) and intraoperative (blue) intra-fiducial distances, (b,d) green arrows point to direction of applied boundary conditions to inferior (I) and superior(S) breast faces highlighted in green.

Fig. III.8(a,c) where the preoperative intra-fiducial distances (red arrows) are larger than the intraoperative intra-fiducial distances (blue arrows). One relatively simple approach to correction is to perform a principal component analysis (PCA) on the difference vector between the co-registered fiducial points to determine the direction in which the largest deformation has occurred. PCA is performed after the displacement field from the first model solve (Section III.4.3.4) has been applied to the preoperative FE mesh and re-registered using the new locations of the preoperative fiducials. The largest distance vector between the gravity transformed preoperative and intraoperative intra-fiducial locations was used to approximate the magnitude of stretching/compression. Being consistent with a simple deployment strategy, the approximated displacement application was then distributed evenly among two control surfaces, as can be seen in Fig. III.8(b,d). The proposed registration method requires only two model solves, providing a fast correction strategy that can

be readily adapted in the operating room. Given the nature of breast deformation and the reduced domain of the breast analyzed, this initial realization is purposefully designed to be work-flow friendly, operationally robust, and constrained to establish a baseline understanding of efficacy. In the discussion below, avenues for improvement are suggested.

III.4.4 Registration Assessment

Surface markers were used to quantify registration accuracy by calculating the root mean square fiducial registration error (FRE). FRE is a measure of overall misalignment between fiducials and captures fiducial localization errors as well as nonrigid movements. It is important to note that fiducial location differences between image and physical space were not used as direct displacement boundary conditions in the model, but only as a measure of fit with respect to applied deformations from gravity-induced changes and inferior-superior control surfaces. With respect to subsurface targeting accuracy, tracked ultrasound image contours of the tumor were compared to their registered preoperative counterpart. More specifically, the centroid location of the preoperative segmented tumor is mapped by the process shown in Fig. III.7 and compared to the centroid location of the appended 3D tracked iUS tumor contours as shown in Fig. III.6. The centroid of a finite number of points was computed as follows:

$$C = [C_x, C_y, C_z] = \frac{\sum_{i=1}^{k} [P_{ix}, P_{iy}, P_{iz}]}{k} \tag{III.4}$$

where k is the number of points in the domain and P_i is a point in space. Using equation III.4, The Euclidean distance ($l_2 - norm$) between the intraoperative tumor centroid ($C_{intraop}$) and preoperative tumor centroid (C_{preop}) was used to measure target registration error: Centroid Difference= $||C_{intraop} - C_{preop}||$.

III.5 Results

III.5.1 Patient 1

The initial rigid alignment of the synthetic skin fiducials for patient 1 yielded an FRE 7.5 mm. Figure III.9(a-c) show results from the rigid registration. The tumor centroid difference between the mapped preoperative and intraoperative states before ultrasound probe compression correction of the intraoperative tumor was 7.5 mm. After probe-to-tissue compression compensation, the tumor centroid difference was 6.5 mm. The iterative closest point registration of the intraoperative and preoperative chest-walls revealed that negligible rotation of the torso occurred for patient 1. Therefore, a gravitation body force was not applied. Principal component analysis of the difference in preoperative and intraoperative fiducial locations revealed a vector supporting approximately 20 mm maximum intra-fiducial distance which its largest component reflective of

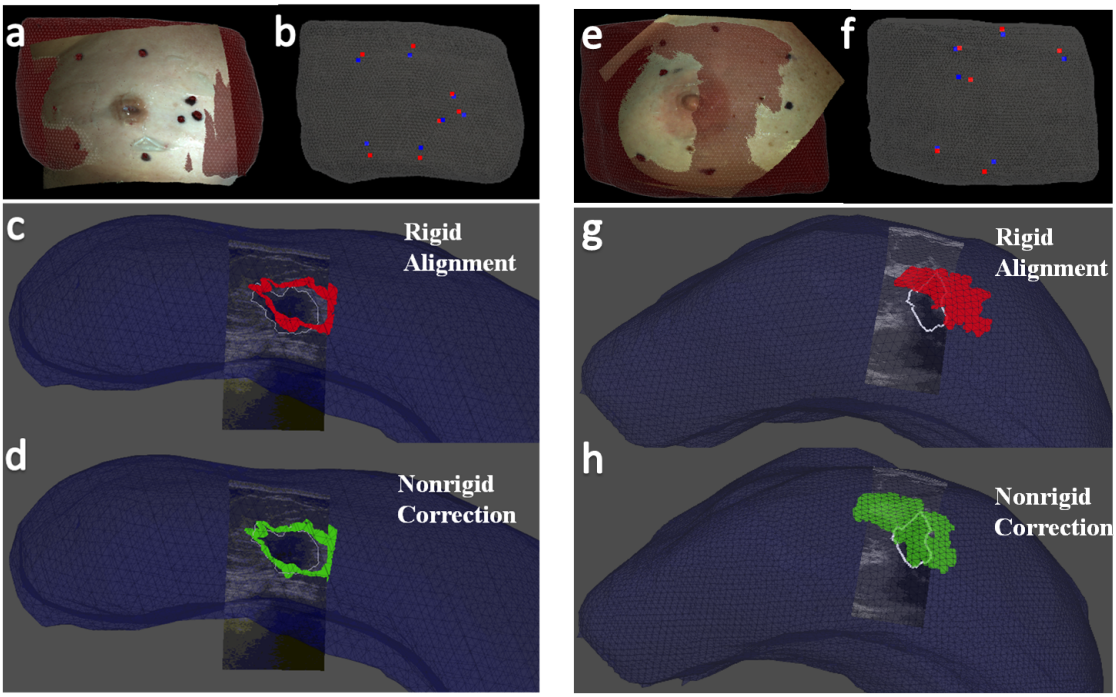

Figure III.9: Patient 1(a-d) and Patient 2 (e-h). (a,e) co-registered textured point cloud and preoperative mesh. (b,f) co-registered preoperative fiducials (red) and intraoperative fiducials (blue). (c,g) intraoperative ultrasound image with white tumor contour overlaid on preoperative rigid aligned tumors in red. (d,h) intraoperative ultrasound image with white tumor contour overlaid on preoperative nonrigid corrected tumors in green.

deformation was along the inferior-superior axis. The difference in intra-fiducial distances can be visualized in Fig. III.8a where the red arrows point to preoperative fiducials and blue arrows point to intraoperative fiducials. This maximum intra-fiducial distance difference was distributed evenly among the two control surfaces. A 10 mm displacement vector was applied to each node on the inferior and superior breast surfaces (green surface shown in Fig. III.8b). The green arrows in Fig. III.8b show the direction of the applied displacements. Using these boundary conditions to drive the elastic model, the nonrigid corrected FRE was 2.9 mm and the deformation corrected tumor centroid difference was 5.5 mm. In Fig. III.9d, we can observe the improved alignment between the MR-rendered tumor and an ultrasound-visible counterpart (white contour) for patient 1.

III.5.2 Patient 2

Initial rigid alignment of the synthetic skin fiducials for patient subject 2 returned an FRE of 8.8 mm. Fig. III.9(e-g) shows results from the rigid registration. The tumor centroid distance between mapped preoper-

ative and intraoperative states before ultrasound compression compensation of the tumor contours was 14.7 mm. The tumor centroid distance after probe-to-tissue compensation was 12.5 mm. Following gravitational direction correction, the FRE improved negligibly to 8.5 mm and with a more considerable correction to the tumor centroid distance decreasing to 8.4 mm. As anticipated, principal component analysis following gravity-induced deformation compensation revealed that the largest deformations occurred along the patient's inferior-superior axis. The largest difference in the intra-fiducial distances was 50 mm. Red and blue arrows in Fig. III.8c show the largest difference in preoperative and intraoperative intra-fiducial distances, respectively. The maximum intra-fiducial distance difference was distributed evenly among the two control surfaces. The green arrows in Fig. III.8d point to the direction of applied displacement boundary conditions with a 25 mm displacement applied at each breast face (highlighted green surface in Fig. III.8d). The nonrigid correction resulted in an FRE of 7.4 mm and tumor centroid distance of 5.4 mm. In Fig. III.9h, we can observe the improved alignment between MR-rendered tumor and the ultrasound-visible counterpart (white contour) for patient 2.

III.6 Discussion

We have presented two patient subjects as an initial investigation towards the realization of a supine image guided surgical platform. In general, the results show that initial rigid alignments are not sufficient and a nonrigid correction is necessary to obtain a clinically relevant image-to-physical alignment. In each case, arm movement between the preoperative and intraoperative patient setups caused a change in stretch to the breast tissue along the patient's inferior-superior axis. Tissue deformation exerted by the ultrasound probe required correction to improve the fidelity of using tracked ultrasound images of the tumor as a means to assess subsurface target registration error. In this study, a somewhat "open-loop", i.e. non-iterative, correction strategy was used in that an initial fiducial registration error was analyzed, body forces and boundary condition were derived, a model was executed, and finally a nonrigid correction was provided. While arguably a coarse nonrigid deformation correction approach, the results are encouraging and speak to the promise of supine image-guided breast surgery. In the future, an iterative optimization strategy will be developed to find the best correction possible driven by all of the information available intraoperatively. Options for additional data already exist. The corrections shown in Fig. III.9 are driven by synthetic fiducial error. This is an admittedly sparse source of data to drive the correction process and other possibilities exist in our approach. For example, while not used in this work, the laser range data shown in Fig. III.5 could serve within a shape conformity metric and employed as a constraint to the nonrigid registration framework.

Several sources of error may contribute to the reported registration inaccuracy. The tracking error of our system has been reported as sub-millimetric for passively tracked rigid stylus bodies (Glossop, 2009).

However, multiple reference targets were attached on range-based targeting devices (laser range scanner and ultrasound). Our tracked laser range scanner has been characterized previously at 2.2 +/- 1.0 mm (Pheiffer et al., 2012) although its use in this particular work was minimal. With respect to the tracked ultrasound imaging, in studies not reported here we have found our average target registration error to be 1.5-2.5 mm in typical tracking experiments (Pheiffer et al., 2014). It is difficult to predict how these errors will combine due to the nature of the registration process. More specifically, our registration approach samples both far-field (chest wall) and near-field (synthetic fiducials) structures which likely constrains internal target error; more study is needed.

Other sources of error between MR-localized fiducial and co-localized ink markings in physical space could be present. While some compensation for iUS error was performed, the validation metrics themselves still have some error. The contour digitization of the tumor using tracked ultrasound may not represent a comprehensive digitization of tumor volume and as a result could produce discrepancies of the tumor volume centroid as compared to its preoperative counterpart. In this study, care was taken to acquire ultrasound images of the tumor in orthogonal planes and at multiple angles to best digitize the whole tumor volume. Despite this care, it is unlikely that the measurement is as rigorous as its tomographic counterpart in MR. Another source of error is our use of a linear elastic model for the nonrigid correction of breast tissue. While small-strain approximations are likely violated, we have found linear models to behave reasonably well in such gross nonrigid alignment procedures. In other work (Rucker et al., 2014) , we have compared linear and nonlinear approaches (linear vs co-rotational finite element approaches) with similar registration problems. The observed differences between these models usually have been quite modest when compared to gross misalignments and instrument error. While all of these errors need further characterization, the results in Fig. III.9 are difficult to discount. In each we see a marked improvement in alignment between ultrasound-visualized intraoperative tumor contour and the preoperative tumor.

III.7 Conclusion

The work reported herein establishes a preliminary realization of an image guided breast surgery approach using supine MR images. A workflow friendly alignment procedure using rigid and nonrigid registration methods is proposed and preliminary data in two patients is reported. The two cases represent a reasonable extent of the configurations possible during image-guided lumpectomy with the first patient (small breast volume) not experiencing gross volumetric misalignment after rigid registration, and the second (large breast volume) showing large shifts of the subsurface tumor target. In each, our investigational correction methodology showed considerable improvement in alignment both in quantitative metrics as well as visual overlays. To our knowledge, this work represents the first comprehensive image guided breast surgery platform using

supine MR and nonrigid model-based registration methods that has been tested under appropriate in vivo clinical conditions with subsurface target registration errors being reported using echogenic tumors. The results are very encouraging at this early stage and many avenues for future work to improve guidance alignment are possible.

CHAPTER IV

Future Work

The components of an image guidance system for breast cancer surgeries and the data needed to generate a corrected alignment of preoperative data to surgical space have been characterized in Chapters II and III. An arguably coarse initial nonrigid model correction was developed to show feasibility. The next obvious progression of this work is to improve the model approach for nonrigid correction. Several approaches can be identified to improve the nonrigid registration framework. A more generalized nonrigid correction is necessary for a readily adapted nonrigid correction strategy in the OR. This could include the use of an iterative optimization to find the best fit driven by all available digitized intraoperative data. Currently, the textured point cloud from the laser range scanner is not being used to constrain or drive the nonrigid registration. The next iteration of the model based nonrigid correction should incorporate the wealth of surface information that is generated by the laser range scan. Furthermore, the chest wall contours could provide a constraint to the optimization by anchoring the model chest wall nodes to the intraoperative chest wall contours. To get an idea of how chest wall alignment can be implemented, Fig. IV.1 shows the chest wall data available for the preoperative (Fig. IV.1b) and intraoperative (Fig. IV.1a) states. Fig. IV.1c shows a rigid registration between the preoperative chestwall model and the tracked ultrasound digitized intraoperative chestwall contours.

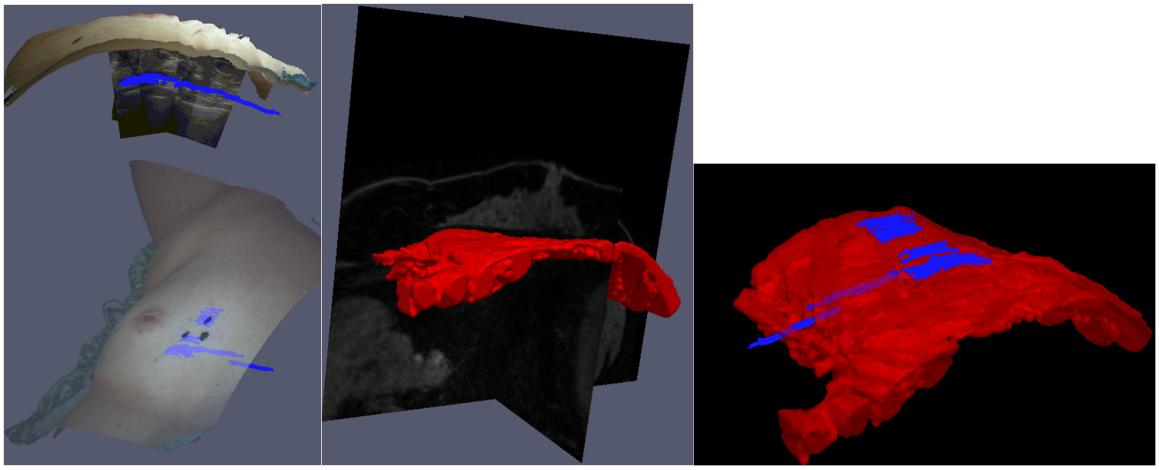

(a) (b) (c)

Figure IV.1: (a) Top: Ultrasound images of the chest wall with chest wall contours shown in blue rendered below the LRS in physical space. Bottom: transparent overlay of the LRS showing ultrasound contours of the chest wall in blue. (b) Segmentation of the preoperative chestwall from the MR image volume. (c) Rigid registration of the preoperative chestwall (red) to the intraoperative tracked ultrasound digitized chest wall contours (blue)

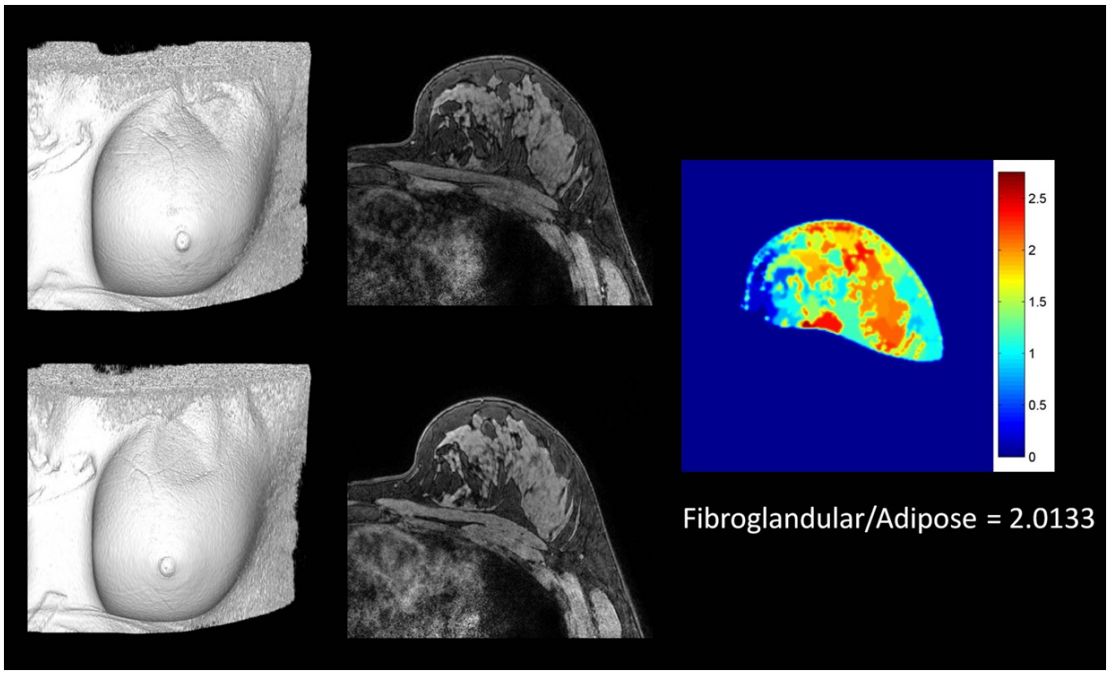

Figure IV.2: MIE result for a healthy volunteer. The far left panel contains volume renders of the volunteer breast, the middle panel displays structural images of the breast. The top two images represent the undeformed (or fixed) state while the bottom two images represent the deformed (or moving) state. The far right image shows an elasticity map containing the resulting elasticity ratios.

Current preoperative models are made up of a homogeneous mesh with only one material property. Another avenue of exploration that could potentially improve the nonrigid correction model is to use a heterogeneous mesh consisting of glandular tissue, adipose tissue, and tumor based on segmentations of the preoperative supine MRI. Furthermore, one could also populate the model with patient specific biomechanical properties. Preliminary feasibility studies have been performed using modality independent elastography (MIE) (Washington and Miga, 2004; Ou et al., 2008) on both prone and supine MR image volumes. Fig. IV.2 and Fig. IV.3 show the results of MIE for a healthy volunteer and a breast cancer patient, respectively. Fig. IV.4 shows the results of gravity-based supine MIE performed on a healthy volunteer.

In both the prone and supine MIE methods, a fixed (or undeformed) image and moving (deformed/rotated) image is acquired. Next, a finite element biomechanical model iteratively deforms the moving image to match the fixed image while optimizing upon mechanical properties until an image similarity metric is met. The differences in the prone and supine methods include the method of achieving the moving image, the generation of boundary conditions, and the output elasticity values (ratios vs. absolute). In the prone method, an undeformed and deformed image is acquired by inflating an air bladder inside the MR breast coil to deform the breast. In the supine method, the patient is rotated slightly and the breast is allowed to freely move due to the difference in tissue weights under gravity. The former method utilizes the chest wall in each image to

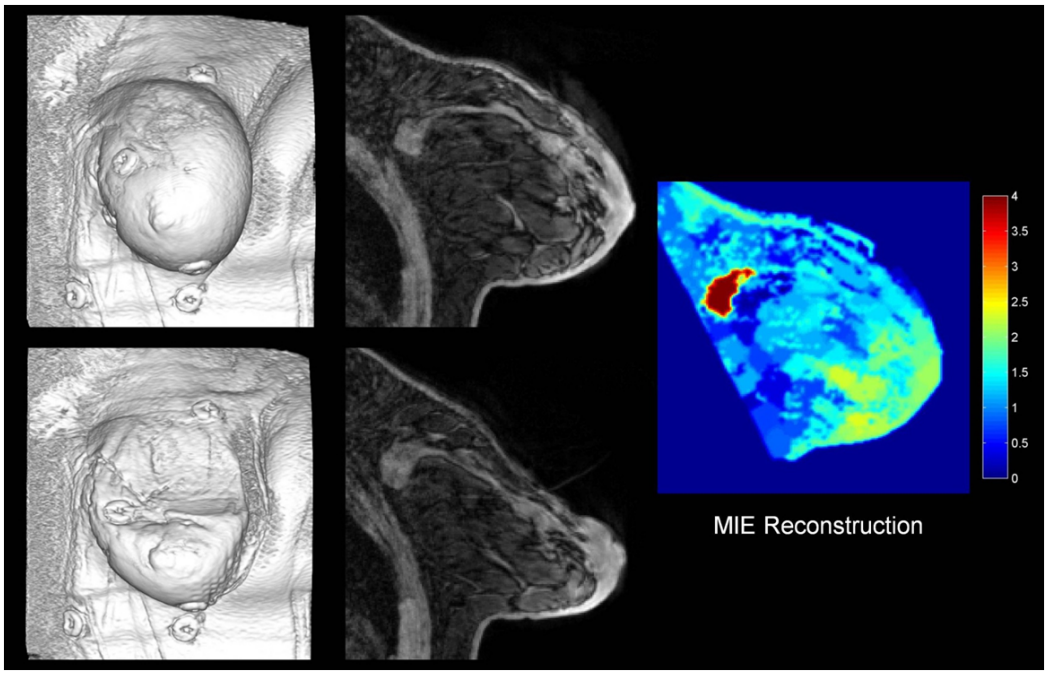

Figure IV.3: MIE result for a patient volunteer. The far left panel contains volume renders of the volunteer breast, the middle panel displays structural images of the breast. The top two images represent the undeformed (or fixed) state while the bottom two images represent the deformed (or moving) state. The far right image shows an elasticity map containing the resulting elasticity ratios.

obtain a gravity differential (similar to Chapter III Section III.4.3.2). The MIE algorithm is then ran with fixed chest wall nodes and stress free nodes elsewhere. The prone method utilizes a nonrigid demons registration between the fixed and moving images to generate boundary conditions. This method has been descried in (Pheiffer et al., 2011). The benefit of the supine method is the fact that the MIE procedure results in absolute quantification of elasticity values whereas the prone MIE procedure results in elasticity ratios. A further area of study would be to develop a method to provide absolute elasticity values in the prone MIE procedure.

Sensitivity of synthetic fiducial placement should be considered and a study to obtain an optimal synthetic fiducial configuration on the breast surface should be conducted. Lastly, the characterization of errors produced by this system and sensitivity analysis of outcome measures due to these errors need to be performed. Overall, this work presents a comprehensive framework for an image guidance system for breast cancer surgeries, with several avenues of future improvement available.

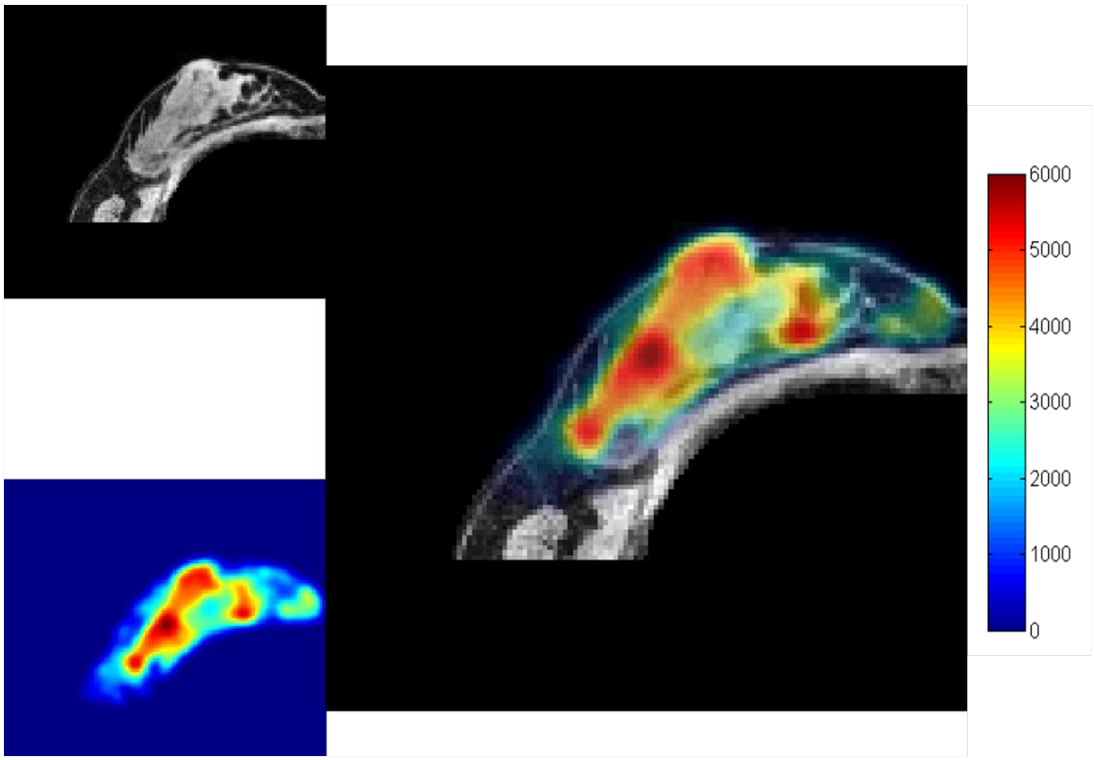

Figure IV.4: Result of MIE using the supine gravity-based deformation technique. The top left image is a axial slice of a structural supine MRI. The bottom left image is the resulting elasticity map. The right image is a fusion with the elasticity map overlaid on top of the structural image. The color bar contains the elastic modulus in units of Pa.

BIBLIOGRAPHY

Abe, M., Kiryu, T., Sonoda, K., and Kashiki, Y. (2011). Magnetic resonance imaging-guided navigation with a thermoplastic shell for breast-conserving surgery. *European Journal of Surgical Oncology (EJSO)*, 37(11):950–955.

Adkisson, C. D., Bagaria, S. P., Parker, A. S., Bray, J. M., Gibson, T., Thomas, C. S., Heckman, M. G., and McLaughlin, S. A. (2012). Which eligible breast conservation patients choose mastectomy in the setting of newly diagnosed breast cancer? *Annals of surgical oncology*, 19(4):1129–1136.

Agarwal, S., Pappas, L., Neumayer, L., Kokeny, K., and Agarwal, J. (2014). Effect of breast conservation therapy vs mastectomy on disease-specific survival for early-stage breast cancer. *JAMA surgery*, 149(3):267–274.

Alderliesten, T., Loo, C., Paape, A., Muller, S., Rutgers, E., Peeters, M.-J. V., and Gilhuijs, K. (2010). On the feasibility of mri-guided navigation to demarcate breast cancer for breast-conserving surgery. *Medical physics*, 37(6):2617–2626.

Allweis, T. M., Kaufman, Z., Lelcuk, S., Pappo, I., Karni, T., Schneebaum, S., Spector, R., Schindel, A., Hershko, D., Zilberman, M., et al. (2008). A prospective, randomized, controlled, multicenter study of a real-time, intraoperative probe for positive margin detection in breast-conserving surgery. *The American Journal of Surgery*, 196(4):483–489.

Behrenbruch, C., Marias, K., Armitage, P., Moore, N., Clarke, J., and Brady, J. (2001). Prone-supine breast mri registration for surgical visualisation. In *Medical Image Understanding and Analysis*.

Besl, P. J. and McKay, N. D. (1992). Method for registration of 3-d shapes. In *Robotics-DL tentative*, pages 586–606. International Society for Optics and Photonics.

Bleicher, R. J., Ciocca, R. M., Egleston, B. L., Sesa, L., Evers, K., Sigurdson, E. R., and Morrow, M. (2009). Association of routine pretreatment magnetic resonance imaging with time to surgery, mastectomy rate, and margin status. *Journal of the American College of Surgeons*, 209(2):180–187.

Braun, M., Pölcher, M., Schrading, S., Zivanovic, O., Kowalski, T., Flucke, U., Leutner, C., Park-Simon, T.-W., Rudlowski, C., Kuhn, W., et al. (2008). Influence of preoperative mri on the surgical management of patients with operable breast cancer. *Breast cancer research and treatment*, 111(1):179–187.

Buxant, F., Scuotto, F., Hottat, N., Noël, J. C., and Simon, P. (2007). Does preoperative magnetic resonance imaging modify breast cancer surgery? *Acta chirurgica Belgica*, 107(3):288.

Carbonaro, L. A., Tannaphai, P., Trimboli, R. M., Verardi, N., Fedeli, M. P., and Sardanelli, F. (2012). Contrast enhanced breast mri: spatial displacement from prone to supine patient's position. preliminary results. *European journal of radiology*, 81(6):e771–e774.

Carter, T., Tanner, C., Beechey-Newman, N., Barratt, D., and Hawkes, D. (2008). Mr navigated breast surgery: method and initial clinical experience. In *Medical Image Computing and Computer-Assisted Intervention–MICCAI 2008*, pages 356–363. Springer.

Carter, T., Tanner, C., Crum, W., and Hawkes, D. (2006a). Biomechanical model initialized non-rigid registration for image-guided breast surgery. *Computational biomechanics for medicine*, page 104.

Carter, T. J., Tanner, C., Crum, W. R., Beechey-Newman, N., and Hawkes, D. J. (2006b). A framework for image-guided breast surgery. In *Medical Imaging and Augmented Reality*, pages 203–210. Springer.

Chandwani, S., George, P. A., Azu, M., Bandera, E. V., Ambrosone, C. B., Rhoads, G. G., and Demissie, K. (2014). Role of preoperative magnetic resonance imaging in the surgical management of early-stage breast cancer. *Annals of surgical oncology*, 21(11):3473–3480.

Conley, R. H., Meszoely, I. M., Pheiffer, T. S., Weis, J. A., Yankeelov, T. E., and Miga, M. I. (2014). Image to physical space registration of supine breast mri for image guided breast surgery. In *SPIE Medical Imaging*, pages 90362N–90362N. International Society for Optics and Photonics.

Davis, K. M., Hsu, C.-H., Bouton, M. E., Wilhelmson, K. L., and Komenaka, I. K. (2011). Intraoperative ultrasound can decrease the re-excision lumpectomy rate in patients with palpable breast cancers. *The American surgeon*, 77(6):720–725.

Del Turco, M. R., Ponti, A., Bick, U., Biganzoli, L., Cserni, G., Cutuli, B., Decker, T., Dietel, M., Gentilini, O., Kuehn, T., et al. (2010). Quality indicators in breast cancer care. *European journal of cancer*, 46(13):2344–2356.

DeSantis, C., Ma, J., Bryan, L., and Jemal, A. (2014). Breast cancer statistics, 2013. *CA: A Cancer Journal for Clinicians*, 64(1):52–62.

Dubuisson, M.-P. and Jain, A. K. (1994). A modified hausdorff distance for object matching. In *Pattern Recognition, 1994. Vol. 1-Conference A: Computer Vision & Image Processing., Proceedings of the 12th IAPR International Conference on*, volume 1, pages 566–568. IEEE.

Ebrahimi, M., Siegler, P., Modhafar, A., Holloway, C. M., Plewes, D. B., and Martel, A. L. (2014). Using surface markers for mri guided breast conserving surgery: a feasibility survey. *Physics in medicine and biology*, 59(7):1589.

Eck, D. L., Koonce, S. L., Goldberg, R. F., Bagaria, S., Gibson, T., Bowers, S. P., and McLaughlin, S. A. (2012). Breast surgery outcomes as quality measures according to the nsqip database. *Annals of surgical oncology*, 19(10):3212–3217.

Eiben, B., Han, L., Hipwell, J., Mertzanidou, T., Kabus, S., Bülow, T., Lorenz, C., Newstead, G., Abe, H., Keshtgar, M., et al. (2013). Biomechanically guided prone-to-supine image registration of breast mri using an estimated reference state. In *Biomedical Imaging (ISBI), 2013 IEEE 10th International Symposium on*, pages 214–217. IEEE.

Esserman, L., Hylton, N., Yassa, L., Barclay, J., Frankel, S., and Sickles, E. (1999). Utility of magnetic resonance imaging in the management of breast cancer: evidence for improved preoperative staging. *Journal of clinical oncology*, 17(1):110–110.

Fancher, T. T., Palesty, J. A., Thomas, R., Healy, T., Fancher, J. M., Ng, C., and Dudrick, S. J. (2009). A woman's influence to choose mastectomy as treatment for breast cancer. *Journal of Surgical Research*, 153(1):128–131.

Fischer, U., Zachariae, O., Baum, F., von Heyden, D., Funke, M., and Liersch, T. (2004). The influence of preoperative mri of the breasts on recurrence rate in patients with breast cancer. *European radiology*, 14(10):1725–1731.

Fisher, B., Anderson, S., Bryant, J., Margolese, R. G., Deutsch, M., Fisher, E. R., Jeong, J.-H., and Wolmark, N. (2002). Twenty-year follow-up of a randomized trial comparing total mastectomy, lumpectomy, and lumpectomy plus irradiation for the treatment of invasive breast cancer. *New England Journal of Medicine*, 347(16):1233–1241.

Fisher, B., Bauer, M., Margolese, R., Poisson, R., Pilch, Y., Redmond, C., Fisher, E., Wolmark, N., Deutsch, M., Montague, E., et al. (1985). Five-year results of a randomized clinical trial comparing total mastectomy and segmental mastectomy with or without radiation in the treatment of breast cancer. *New England Journal of Medicine*, 312(11):665–673.

Fisher, B., Montague, E., Redmond, C., Barton, B., Borland, D., Fisher, E. R., Deutsch, M., Schwarz, G., Margolese, R., Donegan, W., et al. (1977). Comparison of radical mastectomy with alternative treatments for primary breast cancer: a first report of results from a prospective randomized clinical trial. *Cancer*, 39(6):2827–2839.

Fisher, B., Redmond, C., Poisson, R., Margolese, R., Wolmark, N., Wickerham, L., Fisher, E., Deutsch, M., Caplan, R., Pilch, Y., et al. (1989). Eight-year results of a randomized clinical trial comparing total mastectomy and lumpectomy with or without irradiation in the treatment of breast cancer. *New England Journal of Medicine*, 320(13):822–828.

Glossop, N. D. (2009). Advantages of optical compared with electromagnetic tracking. *The Journal of Bone & Joint Surgery*, 91(Supplement_1):23–28.

Golshan, M., Sagara, Y., Wexelman, B., Aydogan, F., Desantis, S., Min, H. E., Vosburgh, K., Jagadeesan, J., Caragacianu, D., Gombos, E., et al. (2014). Pilot study to evaluate feasibility of image-guided breast-conserving therapy in the advanced multimodal image-guided operating (amigo) suite. *Annals of surgical oncology*, 21(10):3356–3357.

Gonzalez, V., Sandelin, K., Karlsson, A., Åberg, W., Löfgren, L., Iliescu, G., Eriksson, S., and Arver, B. (2014). Preoperative mri of the breast (pomb) influences primary treatment in breast cancer: A prospective, randomized, multicenter study. *World journal of surgery*, 38(7):1685–1693.

Han, L., Hipwell, J., Eiben, B., Barratt, D., Modat, M., Ourselin, S., and Hawkes, D. (2014a). A nonlinear biomechanical model based registration method for aligning prone and supine mr breast images. *Medical Imaging, IEEE Transactions on*, 33(3):682–694.

Han, L., Hipwell, J., Mertzanidou, T., Carter, T., Modat, M., Ourselin, S., and Hawkes, D. (2011). A hybrid fem-based method for aligning prone and supine images for image guided breast surgery. In *Biomedical Imaging: From Nano to Macro, 2011 IEEE International Symposium on*, pages 1239–1242. IEEE.

Han, L., Hipwell, J. H., Eiben, B., Barratt, D., Modat, M., Ourselin, S., and Hawkes, D. J. (2014b). A nonlinear biomechanical model based registration method for aligning prone and supine mr breast images. *Medical Imaging, IEEE Transactions on*, 33(3):682–694.

Houssami, N., Ciatto, S., Macaskill, P., Lord, S. J., Warren, R. M., Dixon, J. M., and Irwig, L. (2008). Accuracy and surgical impact of magnetic resonance imaging in breast cancer staging: systematic review and meta-analysis in detection of multifocal and multicentric cancer. *Journal of Clinical Oncology*, 26(19):3248–3258.

Hwang, E. S., Lichtensztajn, D. Y., Gomez, S. L., Fowble, B., and Clarke, C. A. (2013). Survival after lumpectomy and mastectomy for early stage invasive breast cancer. *Cancer*, 119(7):1402–1411.

Hwang, N., Schiller, D. E., Crystal, P., Maki, E., and McCready, D. R. (2009). Magnetic resonance imaging in the planning of initial lumpectomy for invasive breast carcinoma: its effect on ipsilateral breast tumor recurrence after breast-conservation therapy. *Annals of surgical oncology*, 16(11):3000–3009.

Jemal, A., Bray, F., Center, M. M., Ferlay, J., Ward, E., and Forman, D. (2011). Global cancer statistics. *CA: a cancer journal for clinicians*, 61(2):69–90.

Kass, M., Witkin, A., and Terzopoulos, D. (1988). Snakes: Active contour models. *International journal of computer vision*, 1(4):321–331.

Klimberg, V. S. (2003). Advances in the diagnosis and excision of breast cancer. *The American Surgeon*, 69(1):11–14.

Kuhl, C., Kuhn, W., Braun, M., and Schild, H. (2007). Pre-operative staging of breast cancer with breast mri: one step forward, two steps back? *The breast*, 16:34–44.

Landercasper, J., Whitacre, E., Degnim, A. C., and Al-Hamadani, M. (2014). Reasons for re-excision after lumpectomy for breast cancer: Insight from the american society of breast surgeons masterysm database. *Annals of surgical oncology*, 21(10):3185–3191.

Lorensen, W. E. and Cline, H. E. (1987). Marching cubes: A high resolution 3d surface construction algorithm. In *ACM siggraph computer graphics*, volume 21, pages 163–169. ACM.

Lucas, D. J., Sabino, J., Shriver, C. D., Pawlik, T. M., Singh, D. P., and Vertrees, A. E. (2015). Doing more: Trends in breast cancer surgery, 2005 to 2011. *The American Surgeon*, 81(1):74–80.

McGhan, L. J., Wasif, N., Gray, R. J., Giurescu, M. E., Pizzitola, V. J., Lorans, R., Ocal, I. T., Stucky, C.-C. H., and Pockaj, B. A. (2010). Use of preoperative magnetic resonance imaging for invasive lobular cancer: good, better, but maybe not the best? *Annals of surgical oncology*, 17(3):255–262.

McGuire, K. P., Santillan, A. A., Kaur, P., Meade, T., Parbhoo, J., Mathias, M., Shamehdi, C., Davis, M., Ramos, D., and Cox, C. E. (2009). Are mastectomies on the rise? a 13-year trend analysis of the selection of mastectomy versus breast conservation therapy in 5865 patients. *Annals of surgical oncology*, 16(10):2682–2690.

Mortensen, E. N. and Barrett, W. A. (1995). Intelligent scissors for image composition. In *Proceedings of the 22nd annual conference on Computer graphics and interactive techniques*, pages 191–198.

Muratore, D. M. and Galloway Jr, R. L. (2001). Beam calibration without a phantom for creating a 3-d freehand ultrasound system. *Ultrasound in medicine & biology*, 27(11):1557–1566.

Ou, J., Ong, R., Yankeelov, T., and Miga, M. (2008). Evaluation of 3d modality-independent elastography for breast imaging: a simulation study. *Physics in Medicine and Biology*, 53(1):147.

Pallone, M. J., Poplack, S. P., Avutu, H. B. R., Paulsen, K. D., and Barth Jr, R. J. (2014). Supine breast mri and 3d optical scanning: A novel approach to improve tumor localization for breast conserving surgery. *Annals of surgical oncology*, pages 1–6.

Peters, N., Van Esser, S., van den Bosch, M., Storm, R., Plaisier, P., Van Dalen, T., Diepstraten, S., Weits, T., Westenend, P., Stapper, G., et al. (2011). Preoperative mri and surgical management in patients with nonpalpable breast cancer: the monet–randomised controlled trial. *European journal of cancer*, 47(6):879–886.

Pheiffer, T. S., Ou, J. J., Ong, R. E., and Miga, M. I. (2011). Automatic generation of boundary conditions using demons nonrigid image registration for use in 3-d modality-independent elastography. *Biomedical Engineering, IEEE Transactions on*, 58(9):2607–2616.

Pheiffer, T. S., Simpson, A. L., Lennon, B., Thompson, R. C., and Miga, M. I. (2012). Design and evaluation of an optically-tracked single-ccd laser range scanner. *Medical physics*, 39(2):636–642.

Pheiffer, T. S., Thompson, R. C., Rucker, D. C., Simpson, A. L., and Miga, M. I. (2014). Model-based correction of tissue compression for tracked ultrasound in soft tissue image-guided surgery. *Ultrasound in medicine & biology*, 40(4):788–803.

Pleijhuis, R. G., Graafland, M., de Vries, J., Bart, J., de Jong, J. S., and van Dam, G. M. (2009). Obtaining adequate surgical margins in breast-conserving therapy for patients with early-stage breast cancer: current modalities and future directions. *Annals of surgical oncology*, 16(10):2717–2730.

Rajagopal, V., Nash, M. P., Highnam, R. P., and Nielsen, P. M. (2008). The breast biomechanics reference state for multi-modal image analysis. In *Digital Mammography*, pages 385–392. Springer.

Rucker, D., Wu, Y., Clements, L., Ondrake, J., Pheiffer, T., Simpson, A., Jarnagin, W., and Miga, M. (2014). A mechanics-based nonrigid registration method for liver surgery using sparse intraoperative data. *Medical Imaging, IEEE Transactions on*, 33(1):147–158.

Sakakibara, M., Nagashima, T., Sangai, T., Nakamura, R., Fujimoto, H., Arai, M., Kazama, T., Hashimoto, H., Nakatani, Y., and Miyazaki, M. (2008). Breast-conserving surgery using projection and reproduction techniques of surgical-position breast mri in patients with ductal carcinoma in situ of the breast. *Journal of the American College of Surgeons*, 207(1):62–68.

Satake, H., Ishigaki, S., Kitano, M., and Naganawa, S. (2014). Prediction of prone-to-supine tumor displacement in the breast using patient position change: investigation with prone mri and supine ct. *Breast Cancer*, pages 1–10.

Siegler, P., Holloway, C., Causer, P., Thevathasan, G., and Plewes, D. B. (2011). Supine breast mri. *Journal of Magnetic Resonance Imaging*, 34(5):1212–1217.

Sledge, G. W., Mamounas, E. P., Hortobagyi, G. N., Burstein, H. J., Goodwin, P. J., and Wolff, A. C. (2014). Past, present, and future challenges in breast cancer treatment. *Journal of Clinical Oncology*, 32(19):1979–1986.

Sonka, M. and Fitzpatrick, J. M. (2000). Handbook of medical imaging(volume 2, medical image processing and analysis). SPIE- The international society for optical engineering.

Sullivan Jr, J. M., Charron, G., and Paulsen, K. D. (1997). A three-dimensional mesh generator for arbitrary multiple material domains. *Finite Elements in Analysis and Design*, 25(3):219–241.

Sung, J. S., Li, J., Costa, G. D., Patil, S., Van Zee, K. J., Dershaw, D. D., and Morris, E. A. (2014). Preoperative breast mri for early-stage breast cancer: effect on surgical and long-term outcomes. *American Journal of Roentgenology*, 202(6):1376–1382.

Tafra, L., Fine, R., Whitworth, P., Berry, M., Woods, J., Ekbom, G., Gass, J., Beitsch, P., Dodge, D., Han, L., et al. (2006). Prospective randomized study comparing cryo-assisted and needle-wire localization of ultrasound-visible breast tumors. *The American journal of surgery*, 192(4):462–470.

Torre, L. A., Bray, F., Siegel, R. L., Ferlay, J., Lortet-Tieulent, J., and Jemal, A. (2015). Global cancer statistics, 2012. *CA: A Cancer Journal for Clinicians*.

Tozaki, M. and Fukuda, K. (2006). Supine mr mammography using vibe with parallel acquisition technique for the planning of breast-conserving surgery: clinical feasibility. *The Breast*, 15(1):137–140.

Turnbull, L., Brown, S., Harvey, I., Olivier, C., Drew, P., Napp, V., Hanby, A., and Brown, J. (2010). Comparative effectiveness of mri in breast cancer (comice) trial: a randomised controlled trial. *The Lancet*, 375(9714):563–571.

van Esser, S., Hobbelink, M. G., Peeters, P. H., Buskens, E., Van der Ploeg, I. M., Mali, W. P., Rinkes, I. H., and van Hillegersberg, R. (2008). The efficacy of'radio guided occult lesion localization'(roll) versus' wire-guided localization'(wgl) in breast conserving surgery for non-palpable breast cancer: A randomized clinical trial–roll study. *BMC surgery*, 8(1):9.

Washington, C. W. and Miga, M. I. (2004). Modality independent elastography (mie): A new approach to elasticity imaging. *Medical Imaging, IEEE Transactions on*, 23(9):1117–1128.

Yamashiro, N., Tozaki, M., Ogawa, T., Kawano, N., Suzuki, T., Ozaki, S., Sakamoto, N., Abe, S., and Fukuma, E. (2009). Preoperative mri marking technique for the planning of breast-conserving surgery. *Breast Cancer*, 16(3):223–228.

Yushkevich, P. A., Piven, J., Hazlett, H. C., Smith, R. G., Ho, S., Gee, J. C., and Gerig, G. (2006). User-guided 3d active contour segmentation of anatomical structures: significantly improved efficiency and reliability. *Neuroimage*, 31(3):1116–1128.